공학석사 학위논문

Conception and Phase 1 Characterization of an EWOD-based SELEX Platform

전기 습윤 기반 SELEX 플랫폼 구상 및 1 단계 성능 특성 분석

2018 년 08 월

서울대학교 대학원

기계항공공학부

Marie-Angelique SENE

Abstract

Conception and Phase 1 Characterization of an EWOD-based SELEX Platform

SENE Marie-Angelique

School of Mechanical and Aerospace Eng.

Seoul National University

Aptamers are short DNA, RNA, or peptide 3D-shaped structures with the ability to target molecules and proteins for which antibodies are not well suited, with high specificity and affinity. Not only are these 'chemical antibodies' functionally similar to traditional antibodies, but they also present various advantages such as, for instance, their flexible structure, small size, high specificity and stability, which make aptamers a cutting edge way to reach previously unexplored areas of therapeutics and to create treatments that can keep up with the 21st century diseases. These aptamers are developed through an in vitro selection and amplification process named Systematic Evolution of Ligands by Exponential Enrichment (SELEX). This in vitro combination of chemical reactions that synthetically isolates aptamers is performed over several rounds. Nevertheless, some issues such as time consumption, loss of reagents, risks of cross contamination due to constant human intervention during the SELEX process are impeding the widespread application of aptamers in diagnostics and therapy. Thus, there is a need for a microfluidic SELEX platform more rapid, highly efficient, completely automatic and applicable to a wide range of targets.

Inspired by the new advances in MEMS fabrication methods, this thesis presents a novel Electro-Wetting-On-Dielectric (EWOD) digital microfluidic platform with various integrated features (notably heaters, mixers and isolation areas) designed to overcome the obstacles faced in order to create the first EWOD-based SELEX platform. This EWOD platform is designed to carry the whole SELEX process inside a droplet, which is moved from one reaction site to the other while being submitted to the same

reaction conditions then the conventional SELEX process. This droplet movement automation is permitted by an electric interface, which alters the droplet wettability – thus altering its contact angle- on a dielectric surface by varying the electrical potential applied.

This research project is composed of three major axes, two of which are within the scope of this Master thesis requirement : (1) the design and fabrication of the first EWOD digital microfluidic platform for SELEX implementation, (2) the Phase 1 characterization consisting of the conception and fabrication of a highly performant RTD heater/sensor system for a precise thermal control of the SELEX process. The third axe, Phase 2 characterization, involving the run of biological tests and the whole SELEX process on our developed platform was established as a future final objective.

Through the conception and Phase 1 characterization, a highly performant heating/sensing system, based on resistive heating and RTD principles, was developed by altering the electrical properties of ITO with a novel multiple doping method in order to obtain peculiar properties such as a TCR 3 to 4 orders of magnitude higher than documented RTDs.

Keywords: Electro-Wetting-On-Dielectric, Aptamer, SELEX, MEMS, Lab-On-Chip, RTD, TCR
Student Number: 2016-28096

Contents

List of Tables

List of Figures

Chapter 1. Introduction

1.1 Motivation

1.1.1 Challenges

Aptamers present numerous advantages compares to antibodies such as high affinity, specificity, immunogenicity, thermal stability, low cost and high reproducibility. Aptamers can be conjugated to nanoparticles, toxins, siRNAs, chemotherapy drugs among others, which make them cutting edge therapeutic tools for contemporary diseases treatment. Various SELEX protocols for easy and rapid aptamer generation came to light. But in order to achieve rapid high-throughput aptamer selection and to facilitate the integration of aptamers in various applications from research to clinical, it is urgent to develop a rapid, sensitive, compact and low cost alternative to currently available SELEX platforms. Microfluidic chips seems to be a good candidate but SELEX integration into microfluidics presents some challenges specially when it comes to the critical separation step between unbound sequences and aptamer-target complexes.

Unfortunately, one of the main causes slowing down the mainstream use of aptamers is their fabrication technique itself. Indeed, SELEX process present several limitations that cause aptamers to lag behind therapeutic antibodies [1.1].

One limiting factor of SELEX process is its laboriousness, with previous improvements of conventional SELEX, the number of rounds required was reduced to 8-12 rounds to produce highly binding aptamers. Not only is a single round of selection, amplification and purification taking days, but also those steps are not trivial since one must be careful not to cross contaminate the samples thus introducing non-specific binding during selection or bias during amplification [1.2]. Therefore it became necessary to automate the SELEX process, Elligton et al., in order to reduce the user implication in the different steps (i.e. selection, purification and amplification), decided to use robotic workstations [1.3] [1.4], reducing the contamination risks and improving the affinity.

The low throughput of SELEX process is also another limitation that can be overcome by improving the process efficiency. With the conventional SELEX, not only are non-specific interactions with the matrix and other stationary supports a hindrance, but also, filter separations don't have a high resolution power even if they are straightforward. Bowser's group showed that Capillary Electrophoresis can be used for Selection steps [1.5]. First of all, selections are performed in free solution, thus significantly reducing the risks of non-specific interaction with stationary supports eliminating the need for an additional negative selection round. Furthermore, aptamers with low nanomolar dissociation constants can be isolated in no more than two rounds of selection thanks to the increased separation power of Capillary Electrophoresis.

The other largest limitation to the widespread acceptance of SELEX process (thus aptamers) is its time consuming nature. Indeed, SELEX process necessitate weeks or even months to be completed without any guaranty of success. In order to reduce the time necessary for separation after binding, micro beads were used to immobilize target molecules (proteins and small molecules) [1.6] [1.7], that way small molecules can also be used for SELEX. But this method requires a step during which an additional affinity tag or a special functional group is added to the target molecules creating another risk of non-specific binding. Another option: the magnetic bead-based SELEX technique which allows the immobilization of proteins or small molecules targets via an electrostatic interaction or a covalent bond between the affinity tag and the substrate on the functionalized magnetic beads. This method is attractive since magnetic beads are strong candidates for an easy and rapid isolation of aptamer-target-complexes-immobilized beads using a magnetic field [1.8].

Therefore, it is necessary to improve the current SELEX method to increase the efficiency and throughput of the aptamer development system for therapeutics. More precisely, a fully automated system, with micro liter range sample consumption, time consuming and low cost is necessary.

1.1.2 Opportunities

Microfluidic SELEX devices were pointed out as a way to address low efficiency and throughput of aptamer production techniques. Microfluidic chips are versatile, simple and low cost options for POC applications, allowing parallel running reactions in multiple channels. Indeed the use of microfluidic chips for bio essays such as PCR or ELISA is already widespread.

In order to develop a more efficient method to generate aptamers, several techniques for aptamers screening and in microfluidic devices were developed.

For example, a microfluidic chip using sol-gel technology was developed to capture various proteins by their native state in a nanoporous gel without the need of affinity-capture tags [1.9]. This chip can screen high affinity aptamers after several cycles. But the amplification step and elution needs to be done off-chip since microheaters were not incorporated on the chip [1.10]. The other disadvantage is the high production cost and time consumption.

Another alternative is the CE Microfluidic chip [1.11] used to separate aptamer-target complexes from unbound sequences using their mobility differences. This chip high separation efficiency decreased the number of rounds needed to 1-3 rounds. However, when a small molecule is used as the target, the aptamer-target complex velocity is close to that of the unbound sequences making the separation between aptamer-target complexes and unbound sequences difficult.

Magnetic bead-based microfluidic chips were also identified as a rapid, highly efficient, automatic and applicable to a wide range of targets alternative for microfluidic SELEX implementations. Huang et al. also used a microfluidic system and magnetic beads conjugated with C-reactive proteins (CRP) to automatically screen specific aptamers against CRP.

Similarly, Lou et al. developed a Continuous-flow magnetic activated chip-based separation device to select the DNA aptamer that specifically bound to neurotoxin type B in a single round [1.12]. But this device and the CE microfluidic chip are only used for separation and the others steps such as the initial incubation, the amplification and purification need to be conducted off-chip.

Nevertheless, there are a number of limitations linked to the use of magnetic beads such as beads aggregations that may cause blockage in the microchannel; loss of reagents and products during the throughout washing for purification ; and the difficulty to uniformly disperse the magnetic beads throughout the sample for oligonucleotide-target binding.

It is thus necessary to look for another alternative for a efficient and low cost digital microfluidic SELEX platform. Electrowetting on dielectric (EWOD) became nowadays, an emerging technology for LOC development and more precisely, for digital microfluidic applications. This technology allow the programmable manipulation of one or several droplets simultaneously using electrode arrays [1.13]. Various sets of biological essays can be run through an EWOD platform due to its flexibility, therefore, in the recent years efforts have been directed towards the application of EWOD in biological and biomedical research. Furthermore, by concentrating the reaction stage inside a droplet, EWOD technology not only decreases the reagent volume but also it requires low energy consumption, it enables simultaneous control of different droplets with a rapid droplet transportation and it is compatible with detection instruments. Up to now, this technology, that fits for multi-steps laboratory biochemical reactions and essays, was developed for automatic samples preparations (including heating, elution…) but also amplification protocols such as PCR. Nevertheless its potential is yet to be assessed for SELEX implementation. Indeed, among the several steps required in the SELEX process, the challenging one for EWOD automatic implementation is the separation step between unbound sequences and aptamer-target complexes. Indeed in order to come up with a novel bead-less separation method within a droplet, it is necessary to investigate the physical properties in play during binding between sequences and targets in order to use them. Notably, the principle of change of mobility between aptamer-target complexes and unbound sequences used in the CE SELEX development seems to be a valuable candidate.

1.2 Hypothesis

The new developments in micro/nano scale fabrication techniques combined with EWOD technology versality can lead to the conception of the next generation integrated digital microfluidic SELEX devices with improved efficiency, throughput and low cost. This thesis uses the premises that a digital microfluidic

SELEX platform can be developed using EWOD technology, coupled with mobility properties of oligonucleotides depending on their interactions and vertical wetting principles. We hypothesize in this thesis that by using EWOD and wetting transition properties we can not only achieve horizontal manipulation of droplets but also vertical manipulations that will be necessary to conduct our novel separation technique between aptamer-target complexes and unbound oligonucleotides using their mobility differences. Additionally, highly sensitive and performant sets of heaters and sensors are incorporated to the device for a precise thermal control of the SELEX process and low energy consumption actuation.

1.3 Objectives

The above mentioned hypothesis will be proved through the fulfillment of three objectives identified as the major components of our theoretical and experimental approach.

1.3.1 EWOD Digital microfluidic platform development

Our first objective is to fabricate mainly through soft lithography a versatile EWOD digital microfluidic platform on which basic sample manipulation steps such as dispensing, mixing, merging, splitting, but also more complex steps such as heating, thermal control, elution, vertical wetting transitions can be performed. All of this designed within a simple, low cost and user-friendly microfluidic chip with full automation and potential integration with detection instruments for real time monitoring of samples state.

1.3.2 Highly performant Resistance Thermal Detector system

The second objective or Phase 1 characterization is to integrate within that EWOD platform, a highly performant Resistance Thermal Detector heating/sensing system for a precise, highly efficient and low energy consuming thermal control of the several SELEX steps needing heat treatment. Indeed, RTD systems can be easily incorporated into an EWOD system without any additional fabrication steps by converting basic EWOD electrodes into heaters or thermal sensors.

1.3.3 Adaptation of SELEX process on EWOD platform

The final future objective is to run biological tests on the platform notably concerning the vertical wetting transitions necessary for aptamer-target complexes unbound sequences separation. The goal is to ultimately run a whole SELEX process on our single fully automated EWOD digital microfluidic platform.

1.4 Thesis organization

This research project is composed of three major axes, two of which are within the scope of a Master thesis requirement : (1) the conception and development of an EWOD digital microfluidic platform for SELEX implementation, (2) the conception and fabrication of a highly performant RTD heater/sensor system for a precise thermal control of the SELEX process. The third axe which is the run of biological tests and the whole SELEX process on our developed platform was established as a future final objective and more detailed in chapter 6. Prior to the presentation of our work, chapter 2 first establishes background knowledges and the state of the art for aptamers and the SELEX process development. In order to familiarize the reader with EWOD technology and the key theoretical aspects behind it, chapter 3 presents a review of the basics of EWOD technology. In chapter 4, our platform design and fabrication process are presented. Chapter 5 outlines the platform automation technology, its RTD system characterization and the results discussion followed by a summary of the accomplishments and an presentation of the future work in chapter 6.

1.5 References

[1.1] Fitter, S. & James, R. Deconvolution of a complex target using DNA aptamers. J. Biol. Chem. 280, 34193–34201 (2005).

[1.2] Ng, E. W. et al. Pegaptanib, a targeted anti-VEGF aptamer for ocular vascular disease. Nature Rev. Drug Discov. 5, 123–132 (2006).

[1.3] C. J. Cox, P. Rudolph and A. D. Ellington, Biotechnol. Prog., 1998, 14, 845–850.

[1.4] C. J. Cox and A. D. Ellington, Bioorg. Med. Chem., 2001, 9, 2525–2531.

[1.5] Michael T. Bowser, *Analyst*, 2005,130, 128-130

[1.6] Song, K.M., Cho, M., Jo, H., Min, K., Jeon, S.H., Kim, T., Han, M.S., Ku, J.K., and Ban, C. (2011). Gold nanoparticle-based colorimetric detection of kanamycin using a DNA aptamer. Anal Biochem 415, 175-181.

[1.7] Hunho Jo, Seonghwan Lee and Changill Ban, Bio Design l Vol.3 l No.1 l Mar 30, 2015.

[1.8] Joeng, C.B., Niazi, J.H., Lee, S.J., and Gu, M.B. (2009). ssDNA aptamers that recognize diclofenac and 2-anilinophenylacetic acid. Bioorg Med Chem 17, 5380-5387.

[1.9] Ahmad, K.M., Oh, S.S., Kim, S., McClellen, F.M., Xiao, Y., and Soh, H.T. (2011). Probing the limits of aptamer affinity with a microfluidic SELEX platform. PLoS ONE 6, e27051.

[1.10] Weng C-H, Huang C-J, Lee G-B. Screening of Aptamers on Microfluidic Systems for Clinical Applications. *Sensors (Basel, Switzerland)*. 2012;12(7):9514-9529. doi:10.3390/s120709514.

[1.11] S. D. Mendonsa and M. T. Bowser, J. Am. Chem. Soc., 2004, 126, 2021.

[1.12] Lou, X, Qian, J, Xiao, Y., Viel, L., Gerdon, A.E., Lagally, E.T., Atzberger, P., Tarasow, T.M., Heeger, A.J., and Soh, H.T. (2009). Micromagnetic selection of aptamers in microfluidic channels. Proc Natl Acad Sci USA 106, 2989-2994.

[1.13] T. Taniguchi, T. Torii and T. Higuchi, *Lab Chip*, 2002,2, 19-23

Chapter 2. Background and State of the Art

2.1 Aptamers

2.1.1 Potential

Aptamers are short single-stranded deoxyribonucleic acids (ssDNA) or ribonucleic acids (RNA) that go through a selection process for binding to a define target with high affinity and specificity thanks to their ability to fold into complex 3D structures [2.1]. The ssDNA aptamers main 3D structures are (figure 2.1): G-quadruplexes, hairpins (such as stems, loops, bulges...), and pseudoknots [2.2] .

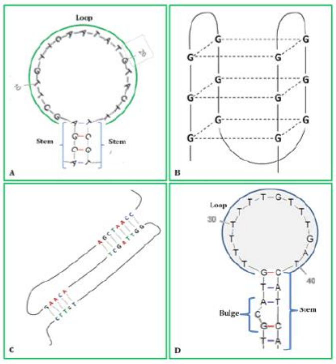

A represents the hairpin structure composed of stem and loop region; B represents the G-quadruplex structure; C represents the pseudoknot structure and; D represents the hairpin structure with a bulge on the stem region. The Figure is reprinted with permission from Dr Shalen Kumar (Victoria University of Wellington, NZ).

Figure 2.1: 3D structures of ssDNA aptamers[2.3]

Up to the recent years, antibodies have been identified as the standard medium for molecular recognition but aptamers are emerging as the new alternative. Indeed, with the same molecular recognition method as antigen-antibody binding, aptamer-target binding happens through the following intermolecular interactions: Van der Waals forces, hydrogen bonding, electrostatic forces and Pi-Pi stacking of “flat-structured” aromatic moieties [2.4]. Aptamers are small-sized, and not only are their binding affinity and specificity similar to those of monoclonal antibodies, but even surpasses them. For instance, aptamers with high target structural specificity and enantioselectivity were developed such as: the theophylline aptamer showing for its cognate ligand an affinity 10 000-fold higher than its affinity for caffeine which differs from theophylline by one methyl group (Figure 2.2) [2.5]. Similarly, an arginine aptamer was developed with a 12 000-fold affinity with L-arginine than with D-arginine [2.6].

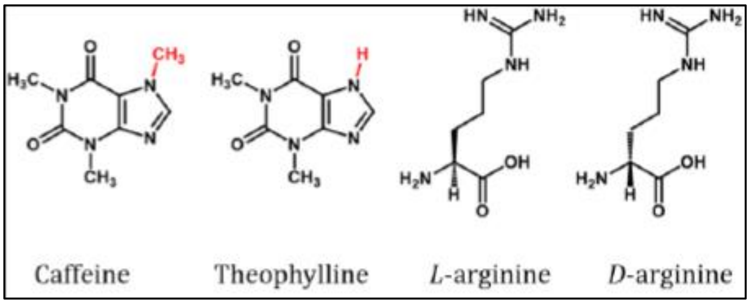

Figure 2.2: Chemical structures of theophylline, caffeine, L-arginine and D-arginine[2.3]

Since aptamers are made of nucleic acids, they are not considered as a foreign agents by the immune agents [2.7]. Thus making aptamers an excellent alternative to antibodies (Table 2.1) and cutting-edge therapeutic tools.

Criteria	Aptamers	Antibody
Basic composition	Nucleotide (four members: A, G, T/U and C)	Amino acid (20 members)
Materials	Nucleic acid (single-stranded DNA or RNA)	• Protein (polymer peptide) • Antibodies consist of two light chains and two heavy chains
Molecular weight and/or size	• 6–30 kDa (20–100 nt) • ~2 nm	• 150–180 kDa • ~15 nm
Secondary structure	• Hairpin, stem, loop, bulge, G-quadruplex or kissing complex	• α-Helix and β-fold
Binding pattern and/or mechanism of action	• Surface recognition • Three-dimensional interactions via van der Waals forces, hydrogen bonding and electrostatic interactions similar to the way antibodies bind to antigen • Reversal of activity via complementary antidote oligonuclotides	• Binding pocket (key and lock model) • Three-dimensional interaction; antibodies recognize epitopes located on the target antigen
Affinity	• High • Multivalent aptamers can confer increasing affinity and additional functions	• High • Affinity between antibody and antigen depends on the number of identical epitopes on the target antigen
Specificity	• High • The aptamer is able to identify single point mutations and conformational isomers	• High • Antigens may have multiple epitopes, which allow different antibodies to bind to the same antigen
Potential targets	• Wide range: ions, organic and inorganic molecules, nucleic acids, peptides, proteins, toxins, viral particles, whole cells, entire organs and live animals	• Limited to immunogenic molecules • No toxins or other molecules that do not cause strong immune responses
Generation and discovery	• *In vitro* SELEX (2–15 selection rounds) • ~2–8 weeks • Aptamer can be selected in hours or days via high-throughput automated SELEX	• *In vivo* biological system • ~6 months or longer
Manufacturing and costs	• Chemical solid-phase synthesis • Controllable and completely *in vitro* procedure • 2 days for milligrams; 2 weeks for grams • No or low risk of contamination • Facile regulatory affairs and cGMP • Low cost for DNA; high cost for long RNA (>60 nt) with special modifications • Costs lowered with the development of new technology	• *In vivo* (animal-based production) • Potential contamination due to cells or animal-based production • 3 months for 5–20 grams • From mammalian cells: high cost • From transgenic plants or animals: low cost
Batch-to-batch variation	• None or low	• Significant
Physical and thermal stability	• Very stable and long shelf-life • Resistant to high temperature (even up to 95 °C) and cycles of denaturation and renaturation • Aptamers can be lyophilized for long-term storage and transport at room temperature	• Unstable and limited shelf-life • Susceptible to temperature (even at room temperature or 37 °C) and irreversible denaturation • Requires refrigeration for storage and transport

Table 2.1: Comparison of nucleic acid aptamers and protein antibodies[2.8]

Up to now, thousands of aptamers have been developed against various targets (Table 2.2) such as metal ions, organic molecules, peptides, proteins, viruses, bacteria, whole cells and even within animal targets [2.8].

Drug name and company	Target	Form and modification	ClinicalTrials.gov identifier (current status)	Condition	Refs
Macular degeneration					
Macugen (pegaptanib sodium) Pfizer/Eyetech	$VEGF_{165}$	• 27-nt RNA • 2′-fluoropyrimidines • 2′-*O*-methyl purines • 3′-inverted dT • 40 kDa PEG	• NCT00021736 (phase II/III, completed)[233] • NCT00040313 (phase II, completed)[234] • NCT00056199 (phase I, completed)[235] • NCT00312351 (phase IV, terminated)[236] • NCT00321997 (phase II/III, completed)[237] • NCT01487070 (phase I, completed)[238] Approved on Dec 2004 in the United States and the European Union for AMD treatment	• AMD • Diabetic macular oedema • Proliferative diabetic retinopathy	14,15, 154
ARC1905 Ophthotech	C5	• 38-nt RNA • 2′-fluoropyrimidines • 2′-*O*-methyl purines • 3′-inverted dT • 40 kDa PEG	• NCT00709527 (phase I, completed)[239] • NCT00950638 (phase I, completed)[240] • NCT02397954 (phase II, completed)[169] • NCT02686658 (phase II/III, recruiting)[170]	• AMD • Idiopathic polypoidal choroidal vasculopathy • Geographic atrophy	168
E-10030 Ophthotech/ Retinal Consultants of Arizona	PDGF	• 29-nt DNA • 2′-*O*-methyl purines • 3′-inverted dT • 40 kDa PEG	• NCT00569140 (phase I, completed)[241] • NCT01089517 (phase II, completed)[178] • NCT02387957 (phase II, recruiting)[242] • NCT02591914 (phase I, ongoing)[243] • NCT01940887 (phase III, recruiting)[181] • NCT01940900 (phase III, ongoing)[180] • NCT01944839 (phase III, recruiting)[179]	• AMD	174,175
Coagulation					
REG1 anticoagulation system (RB006 plus RB007) Regado Biosciences	Coagulation factor IXa	RB006 (drug): • 37-nt RNA aptamer • 2′-ribo purine or 2′-fluoropyrimidine RB007 (antidote): • 17-nt • 2′-*O*-methyl • 40 kDa PEG	• NCT00113997 (phase I, completed)[244] • NCT00715455 (phase II, completed)[189] • NCT00932100 (phase II, completed)[188] • NCT01872572 (phase I, completed)[190] • NCT01848106 (phase III, terminated, clinical hold owing to serious anaphylactic reactions)[191]	• Acute coronary syndrome • Cardiac catheterization (intravenous form) • Coronary artery disease • Percutaneous coronary intervention	183–185, 187
ARC1779 Archemix	A1 domain of von Willebrand factor	• 39-nt DNA • 3′-inverted dT • 2′-*O*-methyl with a single phosphorothioate linkage • 20 kDa PEG	• NCT00432770 (phase I, completed)[195] • NCT00507338 (phase II, terminated)[198] • NCT00632242 (phase II, completed)[245] • NCT00694785 (phase II, withdrawn prior to enrolment)[245] • NCT00742612 (phase II, terminated)[197]	• von Willebrand disease • Thrombotic thrombocytopaenic purpura • von Willebrand disease type 2b • Acute myocardial infarction • Percutaneous coronary intervention • Thrombosis	192–194, 246
NU172 ARCA Biopharma	Thrombin	• 26-nt DNA • Unmodified	NCT00808964 (phase II, unknown, not verified recently)[200]	• Heart disease (for example, used during cardiopulmonary bypass to maintain steady state of anticoagulation)	199

Table 2.2: Nucleic acid aptamers currently in the clinic, AMD, age-related macular degeneration; C5, complement component 5; CCL2, chemokine C-C motif ligand 2; CXCL12, chemokine C-X-C motif ligand 12; dT, deoxythymidine; nt, nucleotide; PDGF, platelet-derived growth factor; PEG, polyethylene glycol; TFPI, tissue factor pathway inhibitor; $VEGF_{165}$, vascular endothelial growth factor isoform 165. [2.8]

2.1.2 Recent progress in therapeutics

There are three different strategies for aptamer exploitation in therapeutics: aptamers can be used as an antagonist to block the interactions of disease-associated targets (protein-protein, receptor-ligand...); or as an agonist to activate the function of target receptors; or, in the case of cell-type-specific aptamers, as a carrier to deliver other therapeutic agents to the target cells or tissues [2.9];[2.10];[2.11] (Figure 2.3).

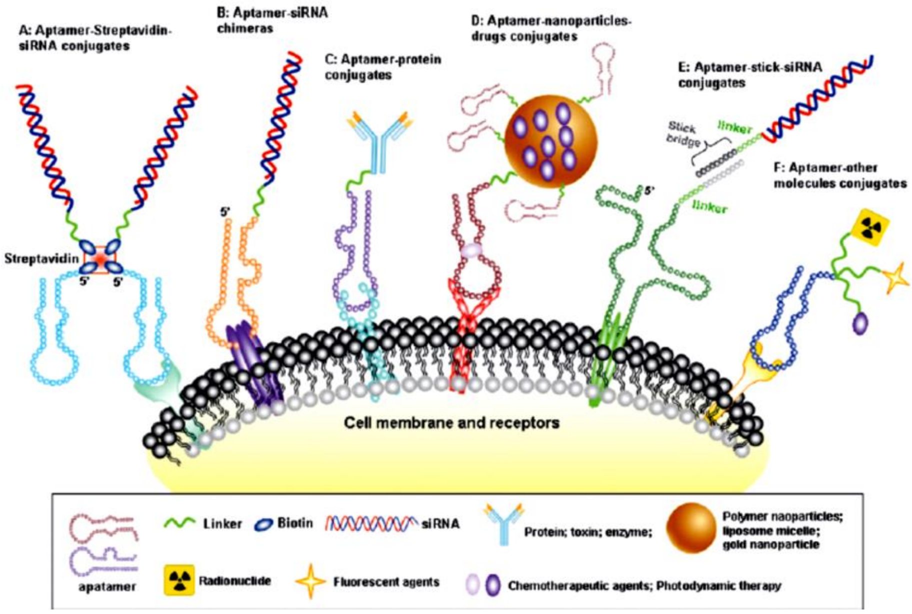

Figure 2.3: Aptamer-mediated cell-type-specific drug delivery[2.12]

2.2 SELEX

2.2.1 History of SELEX

In the early 1990s, aptamers were first developed by two laboratories of Elligton and Szostak [2.13] on one hand, and Tuerk and Gold [2.14] on the other. The technique used to generate these chemical antibodies was named Systematic Evolution of Ligands by Exponential enrichment (SELEX) by Tuerk and Gold.

Following the establishment of the conventional SELEX process, other modified SELEX protocols were introduced (Table 2.3). In 1992, in order to avoid non-specific binding to the environmental components (i.e. agarose matrix), the initial aptamer library is first incubated with the matrix to eliminate the non-specific aptamers, thus conducting a Negative-SELEX [2.15], which increases the aptamer affinity by ten times. Another version of SELEX, called Counter-SELEX [2.16], was introduced two years later which consist of a first aptamer incubation with target analogues before proceeding with the actual target selection round.

Year	SELEX type	References *
1990–1993	Classic, Negative	1,2,5
1994	Counter or Subtractive	6,7
1995	Blended (Covalent), Photoselex (crosslinked), cDNA-SELEX	8–10
1996	Spiegelmer isolation	12
1997	*In vivo*	13
1998	Chimeric	14
1999	Multistage, Cell Specific SELEX(CS-SELEX)	15
2000	Beacon aptamers, Indirect	16–18
2001	Toggle	19,20
2002	Expression cassette	21
2003	Tailored-SELEX	22
2004	CE-SELEX	23
2005	FluMAG	24
2006	TECS-SELEX, NON-SELEX (NCEEM)	25,27
2007	NanoSelection® (nM-AFM SELEX), MonoLEX	28,30
2008	CS-SELEX	31,32
2009	Next-generation SELEX	33
2010	Microfluidic-SELEX, Bioinformatics analyses	36,37,43,44
2011	Multiple-target high-throughput SELEX	38–41

* references correspond to the first report of each type of SELEX; ☐ Setting the ground; ☐ Improving the libraries; ☐ Entering the cell environment; ☐ Regulation and detection; ☐ Updating SELEX with modern Technologies.

Table 2.3: Timeline of emerging modifications of SELEX [2.17]

2.2.2 Conventional SELEX process

SELEX process conventionally involve 5 steps, starting with a DNA or RNA library containing a 20-60 nucleotide random region in between two constant primer regions at the 5′ and 3′ ends (Figure 2.4). That library is then incubated with the target of interest and aptamers with high affinity bind to the target forming an aptamer-target complex. After separation between the unbound sequences and the aptamer-target complexes, elution of the bound aptamers from the complexes takes place. Then amplification of those eluted aptamers is carried on by Polymerase Chain Reaction (PCR) or Nucleic Acid Sequence-Based Amplification (NASBA) for instance, and additional rounds of selection are performed. After obtaining a large number of specific aptamers from a number of rounds, those aptamers are sequenced and their binding properties are evaluated (Figure 2.5).

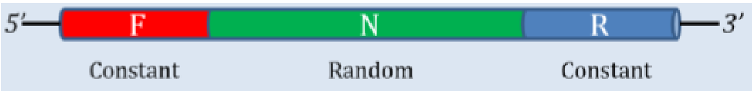

Figure 2.4: Schematic diagram of an aptamer library[2.4]

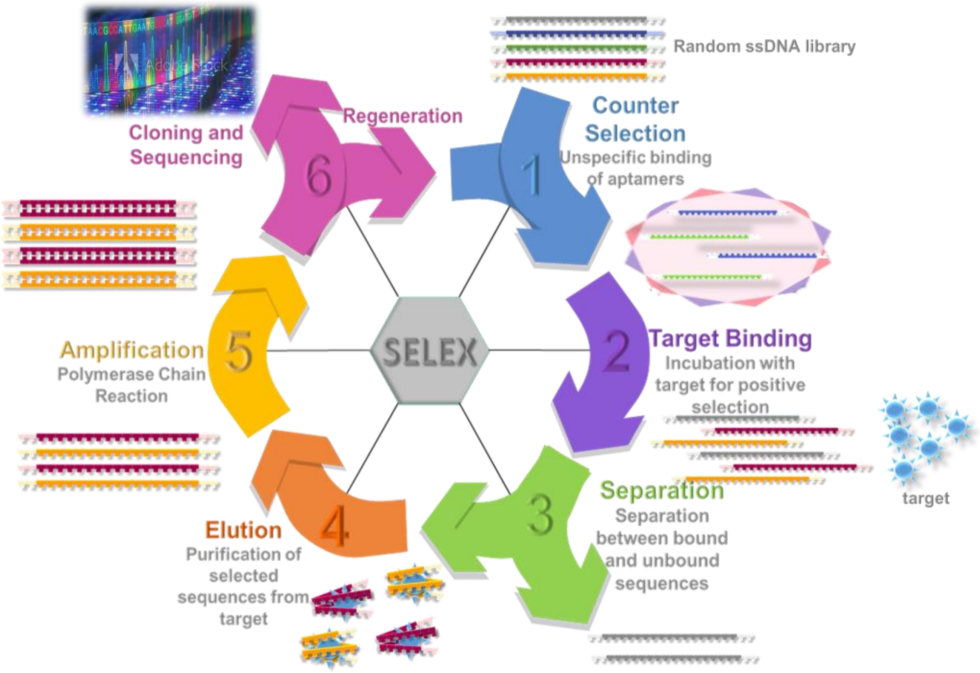

Figure 2.5: Basic principle of SELEX process

For the generation of RNA aptamers, steps such as in vitro transcription and reverse transcription are added to the overall SELEX process. Up to 20 rounds are usually performed for a conventional SELEX process, thus making this approach time and labor consuming. Nonetheless, with the countless SELEX process changes and modifications, it is nowadays possible to develop aptamers in hours instead of the weeks necessary for the first conventional SELEX.

2.2.3 SELEX processes review

Among the most common variants of SELEX processes, we can find Capillary Electrophoresis-SELEX or CE-SELEX [2.18]. This approach differs from the conventional method by the separation of unbound sequences from aptamer-target complexes using their difference in electrophoretic mobility (Figure 2.5). Indeed, unbound sequences have a higher mobility then bound sequences, therefore, the unbound oligonucleotides can pass into the waste area while the aptamer-target complexes remain in the main capillary. Thanks to this method, the number of SELEX rounds can be reduced to 4.

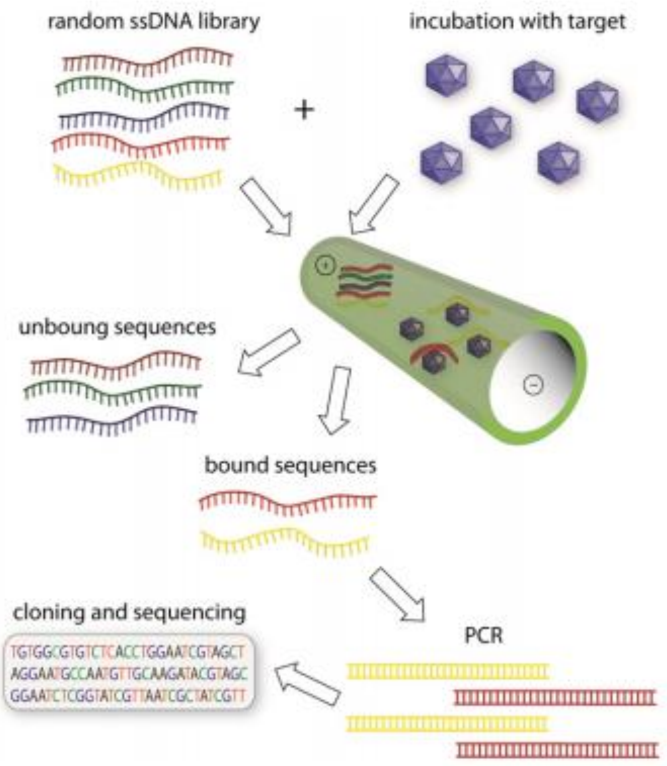

Figure 2.6: Schematic illustration of Capillary Electrophoresis-SELEX [2.19]

In 1997, another variant of SELEX called magnetic bead-based SELEX was introduced [2.20]. For this method, the target protein was coated on magnetic beads thus allowing a magnetic separation between the aptamer-target complexes and the unbound sequences (Figure 2.6).

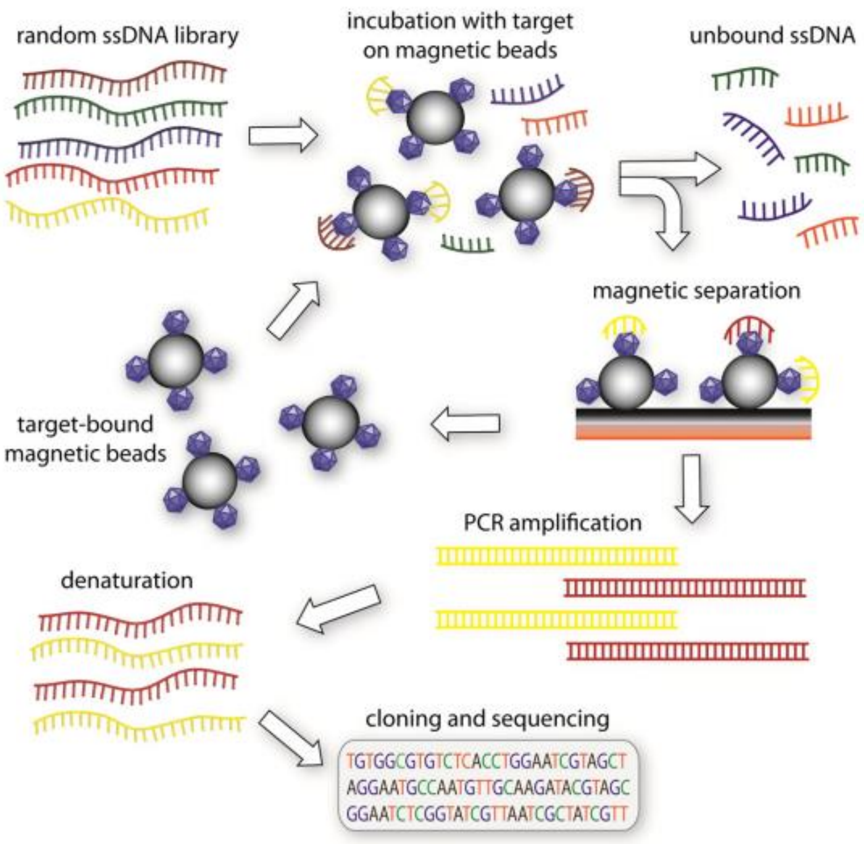

Figure 2.7: Schematic illustration of Magnetic bead-based SELEX [2.19]

Although the above mentioned SELEX processes are carried on for a specific and known target, one variant method does require the prior knowledge of the target : Cell-SELEX (Figures 2.7). Indeed, for this type of SELEX process, target are whole cells, eukaryotic or prokaryotic, and they can generate highly specific aptamers. This approach can necessitate 35 rounds but usually, after 8 to 10 rounds, high affinity aptamers can be obtained. This method is commonly used to generate aptamers against various cell types [2.19].

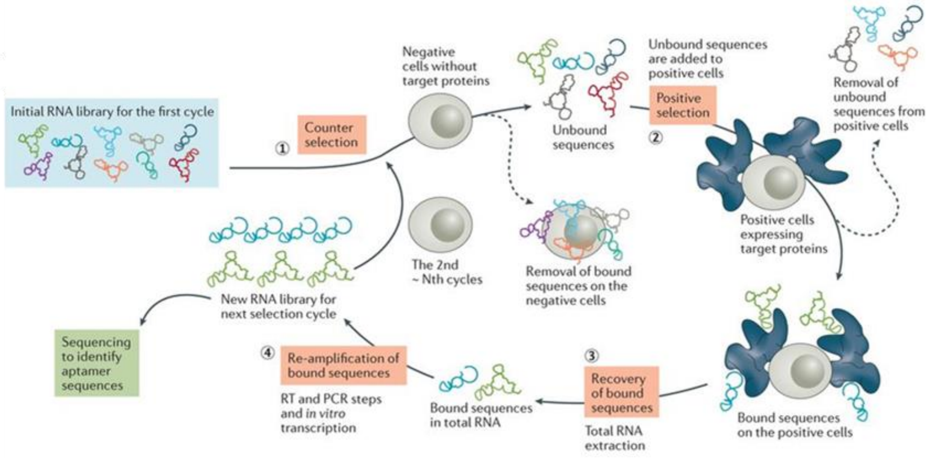

Figure 2.8: Schematic illustration of Whole-cell-based SELEX [2.8]

While SELEX is usually described as an in vitro process, an in vivo SELEX (Figure 2.8) method was developed in 1993 [2.21]. During the first in vivo SELEX process, an infectious combination of HIV-1 DNA genomes with random mutations were transfected into CDT4+ T cells which were then replicated, cloned and sequenced and then used for the SELEX process.

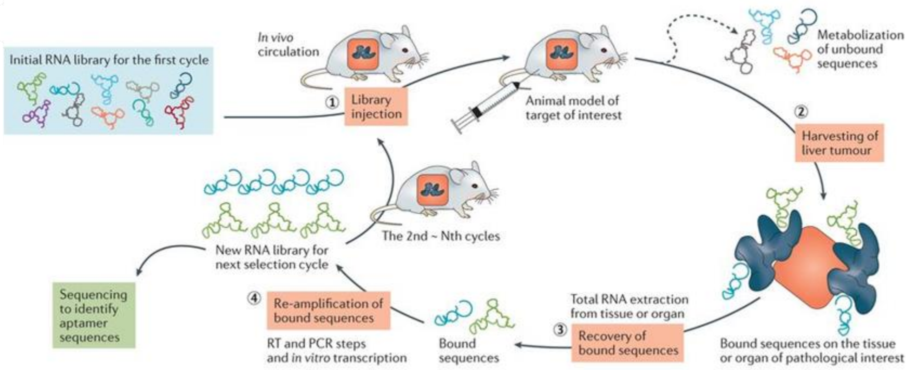

Figure 2.9: Schematic illustration of in vivo SELEX [2.8]

2.3 Microfluidic SELEX implementations

In order to overcome the time and labor consuming nature of the aforementioned SELEX process, several research group have developed rapid, highly efficient and automatable microfluidic SELEX devices. In 2009, a platform that integrates magnetic bead-based SELEX with microfluidics technology, able to generate high-affinity aptamers in one round was developed, named M-SELEX [2.22]. The Overall M-SELEX process (Figure 2.9), for the target Botulinum neurotoxin type A, is organized as follows : the target protein is conjugated to magnetic beads through carbodiimide coupling; then the target and starting library are incubated and separation between unbound sequences and aptamer-target complexes occurs in a CMACS device (Figure 2.10) followed by aptamers amplification.

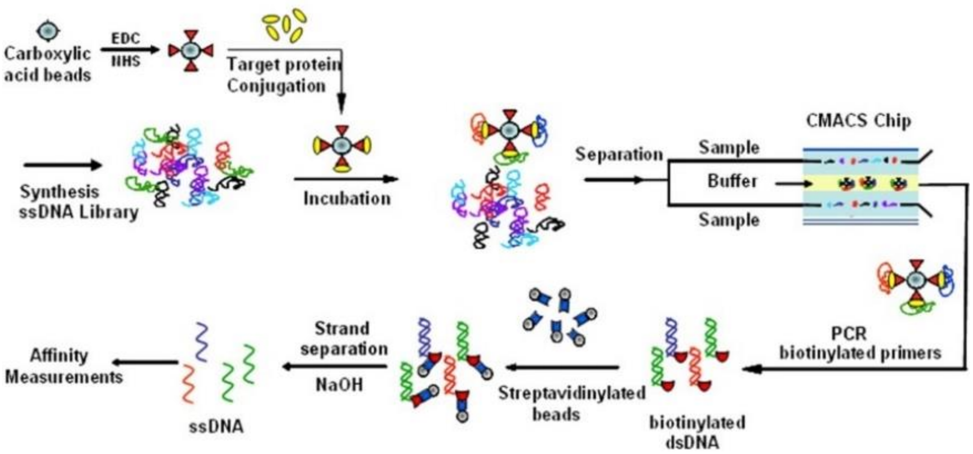

Figure 2.10: Overview of M-SELEX process [2.22]

Inside the CMACS device, the combined mechanical forces along the magnetized Ni strips (external magnet placed in dotted area of Figure 2.10 A) selectively guide the protein-conjugated magnetic beads which are then eluted through the product outlet while the unbound sequences are directed to the waste outlet.

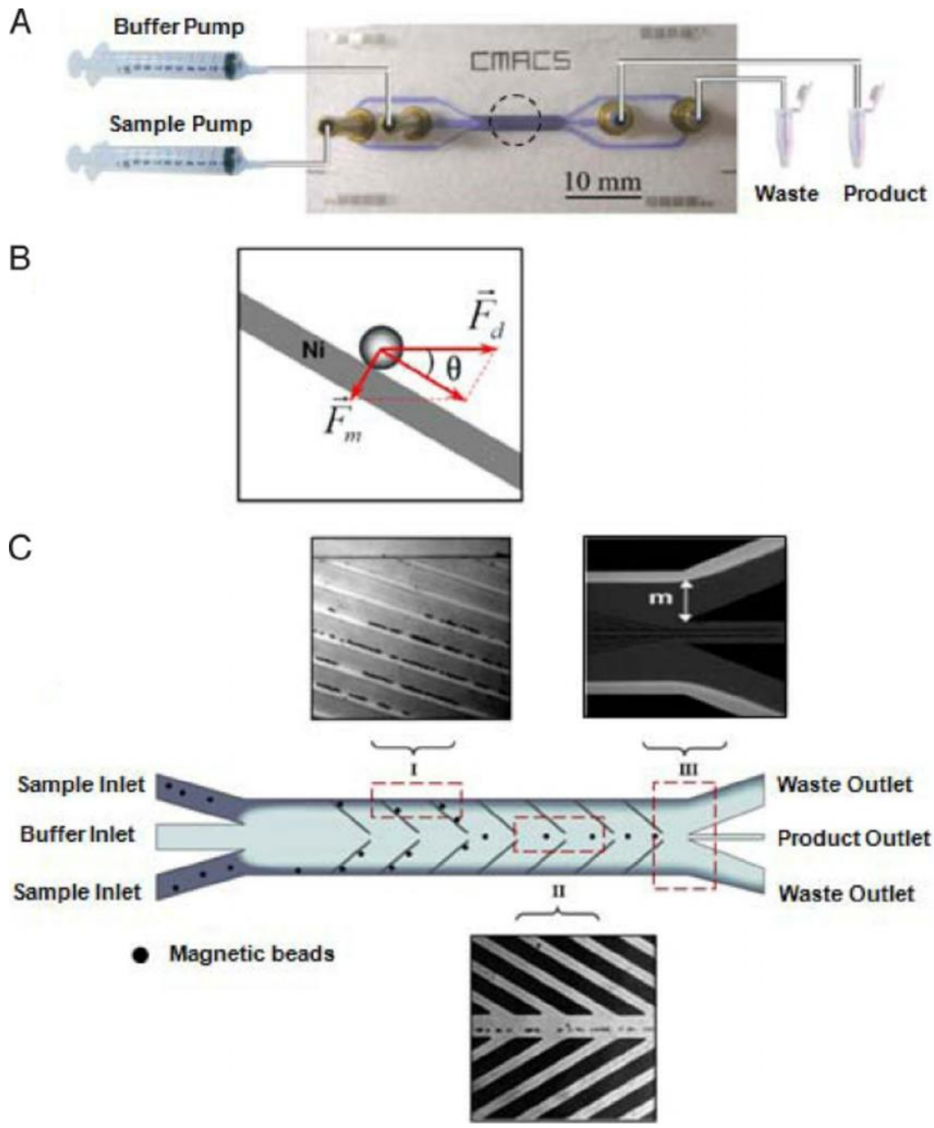

Figure 2.11: Design and physics of the CMACS device[2.22]

Another integrated microfluidic SELEX device using free solution electrokinetics (Figures 2.11) was also introduced in 2017 [2.23]. For this device, an initial library is incubated with target conjugated microbeads for affinity selection, non-binding and weakly binding sequences are washed away through multiple buffer washes. The remaining strong binding oligonucleotides are thermally eluted from the target coated microbeads and transferred to another chamber with amplification microbeads coated with reverse primers, PCR reagents are then introduced and thermal cycles of PCR are launched resulting in amplified copies of the binding sequences hybridized to the beads which are then thermally denatured from the latter and transferred to another chamber for the next selection round.

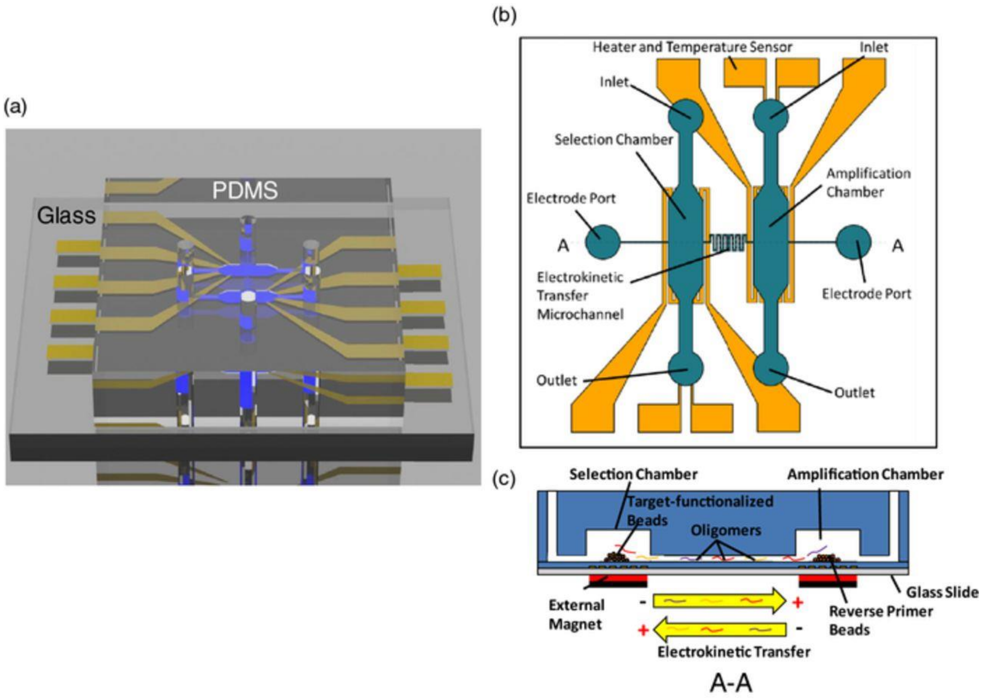

Figure 2.12: Integrated microfluidic SELEX using free solution electrokinetics a) 3D view, b) top schematic view, c)cross-sectional view along line A-A'[2.23]

2.4 References

[2.1] Ellington AD and Szostak JW (1990). "Invitro selection pf RNA molecules that bind specific ligands." Nature 346(6287): 818-822.

[2.2] Feigon J, Dieckmann T and Smith FW (1996). "Aptamer structures from A to zeta." Chemistry & Biology 3(8): 611-617.

[2.3] Hermann T and Patel DJ (2000). "Biochemistry - Adaptive recognition by nucleic acid aptamers." Science 287(5454): 820-825.

[2.4] Li S. (2016). "Selection and Characterisation of single-stranded DNA aptamers for Triclosan", PhD Thesis

[2.5] Jenison RD, Gill SC, Pardi A and Polisky B (1994). "High-resolution molecular discrimination by RNA." Science 263(5152): 1425-1429.

[2.6] Geiger A, Burgstaller P, vonderEltz H, Roeder A and Famulok M (1996). "RNA aptamers that bind L-arginine with sub-micromolar dissociation constants and high enantioselectivity." Nucleic Acids Research 24(6): 1029-1036.

[2.7] Ireson CR and Kelland LR (2006). "Discovery and development of anticancer aptamers." Molecular Cancer Therapeutics 5(12): 2957-2962.

[2.8] Zhou J, Rossi J. Aptamers as targeted therapeutics: current potential and challenges. *Nature reviews Drug discovery*. 2017;16(3):181-202. doi:10.1038/nrd.2016.199.

[2.9] Keefe AD, Pai S, Ellington A. Aptamers as therapeutics. Nat Rev Drug Discov. 2010;9:537–50.

[2.10] Nimjee SM, Rusconi CP, Sullenger BA. Aptamers: an emerging class of therapeutics. Annu Rev Med. 2005;56:555–83.

[2.11] Zhou J, Rossi JJ. Cell-type-specific, Aptamer-functionalized Agents for Targeted Disease Therapy. Mol Ther Nucleic Acids. 2014;3:e169.

[2.12] Zhou J, Rossi JJ. Cell-Specific Aptamer-Mediated Targeted Drug Delivery. *Oligonucleotides*. 2011;21(1):1-10. doi:10.1089/oli.2010.0264.

[2.13] Ellington AD and Szostak JW (1992). "Selection invitro of single strand-DNA molecules that fold specific ligand-binding structures." Nature 355(6363): 850-852.

[2.14] Tuerk C and Gold L (1990). "Systematic evolution of ligands by exponential enrichment - RNA ligands to bacteriophage-T4 DNA-polymerase." Science 249(4968): 505-510.

[2.15] Ellington, A.D.; Szostak, J.W. Selection in vitro of single-stranded DNA molecules that fold into specific ligand-binding structures. Nature 1992, 355, 850–852.

[2.16] Jenison, R.D.; Gill, S.C.; Pardi, A.; Polisky, B. High-resolution molecular discrimination by RNA. Science 1994, 263, 1425–1429.

[2.17] Aquino-Jarquin G, Toscano-Garibay JD. RNA Aptamer Evolution: Two Decades of SELEction. *International Journal of Molecular Sciences*. 2011;12(12):9155-9171. doi:10.3390/ijms12129155.

[2.18] S.D. Mendonsa, M.T. Bowser, *In vitro* evolution of functional DNA using capillary electrophoresis, J Am Chem Soc, 126 (2004), pp. 20-21.

[2.19] M. Darmostuk, S. Rimpelova, H. Gbelcova, T. Ruml, Current approaches in SELEX: An update to aptamer selection technology, Volume 33, Issue 6, Part 2, 1 November 2015, Pages 1141-1161.

[2.20] J.G. Bruno, *In vitro* selection of DNA to chloroaromatics using magnetic microbead based affinity separation and fluorescence detection, Biochem Biophys Res Commun, 234 (1997), pp. 117-120.

[2.21] B. Berkhout, B. Klaver, *In vivo* selection of randomly mutated retroviral genomes, Nucleic Acids Res, 21 (1993), pp. 5020-5024.

[2.22] Lou, X, Qian, J, Xiao, Y., Viel, L., Gerdon, A.E., Lagally, E.T., Atzberger, P., Tarasow, T.M., Heeger, A.J., and Soh, H.T. (2009). Micromagnetic selection of aptamers in microfluidic channels. Proc Natl Acad Sci USA 106, 2989-2994.

[2.23] Olsen TR, Tapia-Alveal C, Yang K-A, et al. INTEGRATED MICROFLUIDIC SELEX USING FREE SOLUTION ELECTROKINETICS. *Journal of the Electrochemical Society*. 2017;164(5):B3122-B3129. doi:10.1149/2.0191705jes.

Chapter 3. EWOD Technology

This chapter presents a review of the fundamentals of EWOD technology: in the case of droplet-based microfluidics, single or multiple droplets in contact with dielectric layer are dispensed, transported, mixed, heated… [3.1] by applying DC or AC voltage across the electrodes covered by the dielectric layer. Various EWOD configurations can be used for droplets manipulation such as the closed EWOD configuration or the open EWOD configuration [3.2],[3.3],[3.4]. Thus due to its versality and simple nature, EWOD can be implemented to a wide range of applications such as optical devices such as displays [3.5] and liquid lens [3.6], but also lab-on-a-chips [3.7],[3.8] among others.

Electrowetting on dielectric is the principle describing the change of droplet contact angle by applying a electric potential. Indeed, when an electric potential is applied to the droplet through the dielectric layer, the contact angle at the interface between it and the dielectric layer decreases [3.9].

3.1 Theory

Gabriel Lippmann first discovered the phenomenon know as electrocapillarity, which is the foundation of electrowetting [3.10]. Electrowetting mainly consist of the modification of the wetting properties of a solid conductive substrate, thus the movements of partially wetting droplets above it, by applying a voltage [3.11]. This application of an external electric potential allows the manipulation of droplets by modifying their solid/liquid interfacial tension, thus their contact angle.

Electrowetting evolved to EWOD after Berge added a thin dielectric layer in order to overcome breakdown issues such as the electrolytic decomposition of droplets [3.12],[3.13]. Figure 3.1 represent the basic setting of an EWOD device which is composed of a sessile droplet, a planar substrate with a dielectric layer on top and a voltage source.

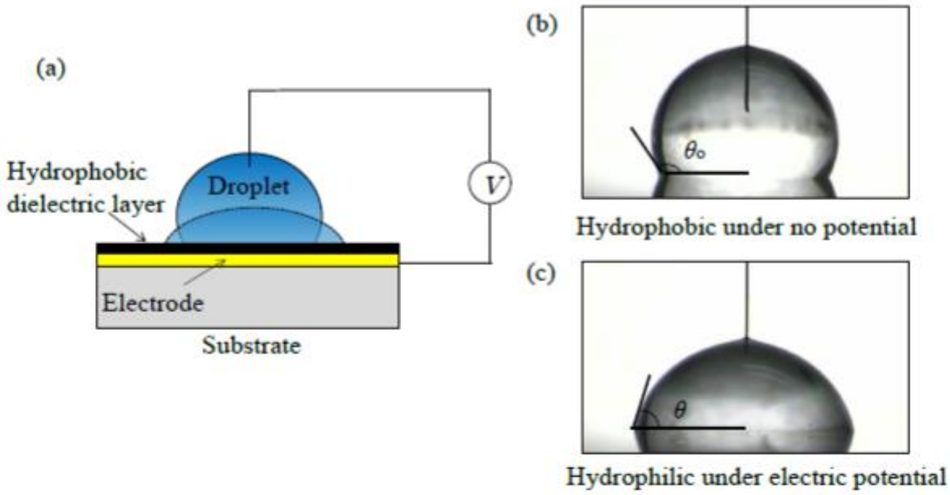

Figure 3.1 : Basic principle of an EWOD setup. a) EWOD configuration. b) droplet at 0V. c) droplet under electric potential [3.9]

Figure 3.1 b) and c) illustrate the change in contact angle resulting from the change of substrate wetting properties. Figure 3.1 b) shows a sessile droplet on a hydrophobic surface without any electric potential applied to it, therefore, in this configuration, the droplet contact surface is minimized. When a electric potential is applied, creating a potential difference between the droplet and the electrode under the dielectric layer as in Figure 3.1 c), the substrate wettability increases causing the droplet to spread across the surface. This EWOD principle is governed by the Lippmann-Young equation [3.14] (1) :

$$\cos\theta = \cos\theta_o + \frac{c}{2\gamma_{LG}} V^2 \qquad (3.1)$$

where θ_o and θ are respectively the initial contact angle when the applied voltage

V to the dielectric layer is zero and when V is different from zero, c is the capacitance per unit area (F/m^2) of the dielectric layer, and γ_{LG} is the interfacial tension between air and water (~0.072 N/m).

Based on the Lippmann-Young equation, the electrostatic energy stored in the capacitor (composed of droplet base surface, dielectric and conductive substrate since fringe effects are neglected [3.15]) caused the change of contact angle. Furthermore, the droplet advancing and receding can be precisely controlled since the change in the contact angle cosine is directly proportional to the applied voltage. By applying a voltage to the EWOD system, an electric field (caused by the induced charge stored near the contact line), with a component parallel with the solid/liquid interface direction, generates an horizontal electrochemical force per unit length (N/m) from the droplet towards the ambient. Therefore, the initial contact angle decreases macroscopically becoming θ, but the microscopic contact angle θ_o does not change [3.15]. Thus, it is important to note that the term contact angle is actually referring to a macroscopic contact angle [3.16] or apparent.

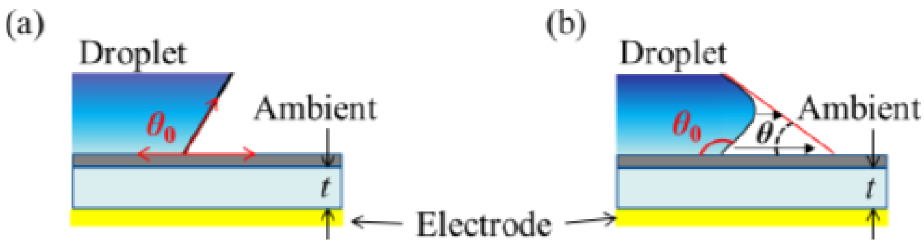

Figure 3.2 : Diagrams of electrowetting basics in microscopic scale. Young's contact angle θ_o at V = 0 (a) and contact angle at V ≠ 0 (b). Young's contact angle unchanged even if electromechanical force is acting toward ambient from droplet.[3.9]

Moreover, the specific capacitance for a dielectric of thickness t is :

$$c = \varepsilon_0 \varepsilon_d / t \tag{3.2}$$

where ε_o is the permittivity of free space (8.85419×10^{-12} F/m), ε_d is the dielectric constant of the dielectric layer.

3.1.1 Static electrowetting : Lipmann-Young law

At microscale, due to peculiar capillarity and surface tension laws, droplets tend to appear as a valuable candidate for microfluidics manipulations. For instance, micro range droplets tend to take a spherical shape at their initial state (i.e. without electric actuation) while bigger droplets tend to fall flat on the surface. When it comes to static electrowetting, the droplet can take two shapes mainly due to two forces: the surface tension and gravity. In the case where gravity is negligible in front of surface tension (microscale) the droplet will be spherical. On the other hand, if both gravity and surface tension act upon the droplet (force balance), then the latter will be flattened [3.16].There are two ways to determine the shape of a droplet. The first method is by using the capillary length or scale length l which is governed by the following equation (3.3) [3.17]:

$$\frac{\Delta P_{Laplace}}{\Delta P_{hydrostatic}} = \frac{\frac{\gamma}{l}}{\rho g l} \tag{3.3}$$

Where γ is the surface tension, ρ the density, and g the gravitational constant. When the hydrostatic pressure and the Laplace pressure are at the same order, it is possible to deduce the capillary length l, thus the droplet shape, with the following equation (3.4) :

$$l \approx \sqrt{\frac{\gamma}{\rho g}} \qquad (3.4)$$

where l is the capillary length. Indeed, if the droplet size is larger than the capillary length, then both gravity and surface tension are applied to the droplet resulting in a flattened shape. But if the droplet size is smaller than the capillary length then the droplet will have a spherical shape.

The second method used to deduct which force is applied to the droplet is based on the Bond number value : if the Bond number is superior to unity, then both the gravitational force and the surface tension are applied to the droplet thus resulting in a flattened shape. On the other hand, if the Bond number is inferior to unity, then only the surface tension forces are considered resulting in a spherical shape. The capillary length expressed in equation (3.4) also gives access to the Bond number which is without dimension. That Bond number is expressed through this equation:

$$B_o \approx \frac{\rho g R^2}{\gamma} \qquad (3.5)$$

where R is the radius of the droplet [3.16].

Additionally, the above mentioned Young equation was derived with the hypothesis that the surface is smooth without any roughness, but in reality, due to imperfections such as chemical residues or particles, even in the case of devices fabricated in the CMOS range clean-room, the surface roughness cannot be completely neglected [3.18]. Therefore, the droplet static wetting properties need to be described taking into account the surface roughness, which corresponds to Cassie and Wenzel wetting models or respectively non-wetting and complete wetting models [3.19] (Figure 3.3). It is important to note that these two models are applicable if the droplet dimension is sufficiently large compared to the surface roughness [3.16].

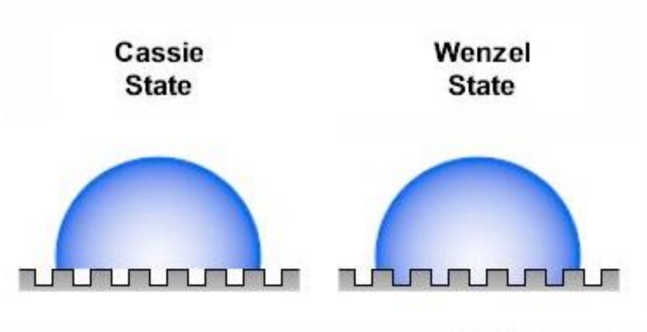

Figure 3.3 : Droplet wetting transitions on a rough surface (a) Cassie state and (b) Wenzel state [3.59]

The non-wetting model or Cassie model (Figure 3.3 a)) represent the state where the droplet rest only on the tips of the surface features leaving some air trapped in the trenches [3.16][3.20]. This state is described by the Cassie-Baxter relation (equation (3.6)) which give the droplet contact angle in Cassie state[3.16] :

$$\cos\theta^* = \sum f_i \cos\theta_i \qquad (3.6)$$

where i represents the different chemical components of the surfaces.

This relation describes the modified wetting properties taking place on a chemically inhomogeneous surface. Indeed, in the case of a microscopically inhomogeneous surface, the cosine of the droplet contact angle is equivalent to the sum of the cosine of the different contact angles of the different chemical components of the surface. On the other hand, the complete wetting state or Wenzel state (Figure 3.3 b)) corresponds to the wetting state in which the droplet wets the surface features completely also filling the trenches thus occupying a greater surface area than in the Cassie state [3.16][3.20]. This state is governed by the Wenzel equation (equation (3.7)) :

$$\cos\theta^* = r\cos\theta \qquad (3.7)$$

Where r is the surface roughness and by definition is greater than 1, θ^* is the droplet contact angle, θ is Young's contact angle. This relation describes a hydrophilic wetting (Figure 3.4 b) top) when the droplet contact angle θ^* is smaller than Young's contact angle θ ; the hydrophobic wetting (Figure 3.4 b) bottom) corresponds to the case where the droplet contact angle θ^* is bigger than Young's contact angle θ [3.16].

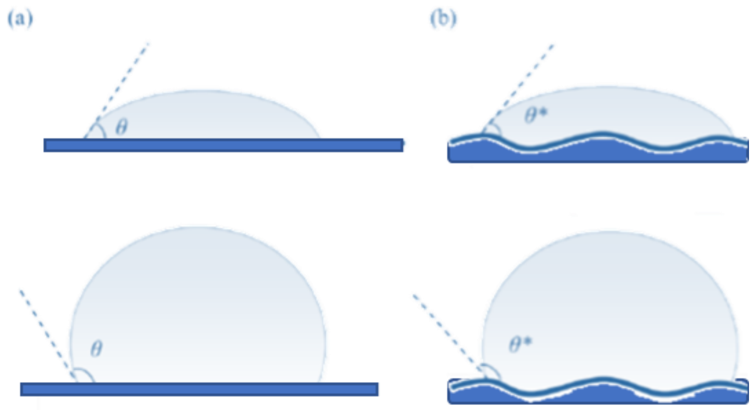

Figure 3.4: Contact of droplet on an ideally flat surface (a) and a rough surface (b) [3.9].

3.1.2 Dynamic electrowetting model

Surface tension forces being dominant at microscale, EWOD technique appears as an excellent method to activate and move droplets since it consist of the modulation of surface tension. In order to induce a lateral transport of the droplet by electrowetting-based micro actuation, interfacial gradient forces are generated by applying an electric potential to only one side of the droplet [3.21]. In order for this droplet micro-actuation to work, it is necessary for the droplet to be big enough to cover not only the center of one electrode but also to overlap all adjacent electrodes [3.22]. That way, when an electric potential is applied to one of the adjacent electrodes, an electromechanical force applied around the contact line will thus induce the droplet movement with around more than 40º contact angle variation on average [3.23].

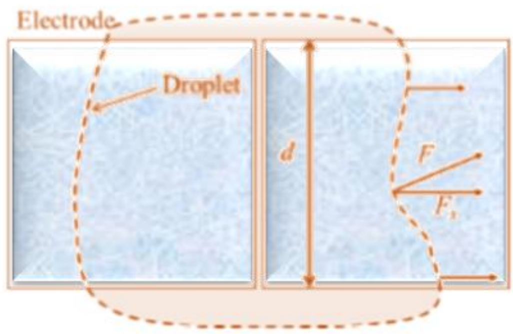

Figure 3.5: Forces at play during droplet electrowetting-based micro-actuation [3.9].

It is also necessary to carefully decide on the electrodes dimensions. Indeed, since the electrowetting-based micro actuation evolves around the Young's contact angle and surface tension forces at the solid/liquid interface, the smaller the electrode, the greater its electrowetting effect will be.

Another important phenomenon to take into account for a successful electrowetting-based micro actuation is the contact angle hysteresis at the contact line [3.25][3.26]. In order to define that contact angle hysteresis, it is necessary to first define the notions of advancing contact angle and receding contact angle. The advancing contact angle is caused by a rise in the applied electric potential which results in the droplet spreading over the actuated surface. If the applied potential is then reduced, the droplet retracts back to its initial position or equilibrium position which results to a receding contact angle. But it is known as an empirical fact that the advancing contact angle is larger than the receding contact angle [3.27], therefore the contact angle hysteresis is defined as the difference between the advancing contact angle and the receding contact angle [3.28]. For instance, the contact angle hysteresis for a DIW droplet in an air medium is between 7º and 9º while the contact angle hysteresis for a DIW droplet in a silicon oil medium is between 1.5º and 2º [3.24].

In the case of a droplet micro actuation using adjacent electrodes (Figure 3.5), it is possible to determine the minimum required voltage for the droplet actuation when there is a contact angle hysteresis. First of all, the x direction component of the capillary force applied on the droplet interface is described as :

$$F_x = d\gamma(\cos\theta - \cos\theta_o). \qquad (3.8)$$

The advancing component and the receding component of the capillary force in the x direction can be deduced by including the contact angle hysteresis α in equation (3.8) :

$$F_x^A = d\gamma(\cos\theta + \alpha)$$

$$F_x^R = -d\gamma(\cos\theta_o - \alpha). \qquad (3.9)$$

By hypothesizing that the contact angle α is neglectable in front of θ and θ_O the previous equations can be written as:

$$\begin{aligned} F_x^A &= d\gamma[\cos\theta - \alpha(\cos\theta + \sin\theta)] \\ F_x^R &= -d\gamma[\cos\theta_o - \alpha(\cos\theta_o - \sin\theta_o)]. \end{aligned} \qquad (3.10)$$

By adding the advancing component and the receding component of the capillary force in x direction :

$$F_x = d\gamma[\cos\theta - \cos\theta_o] - d\gamma\alpha[\cos\theta + \sin\theta - \cos\theta_o + \sin\theta_o]. \qquad (3.11)$$

By injecting the x component of the capillary force (equation (3.11)) in the Lipmann-Young equation in the minimum displacement condition, the following relation can be generated :

$$\frac{d}{2}cV^2 - d\gamma\alpha[\cos\theta + \sin\theta - \cos\theta_o \quad + \sin\theta_o\ ] > 0. \qquad (3.12)$$

Which gives the square value of the minimum required voltage :

$$V^2_{\min} = \frac{2\gamma}{c}\alpha[\cos\theta + \sin\theta - \cos\theta_o + \sin\theta_o\ ] \ (3.13)$$

Leading to the following simplified value of the minimum required voltage or threshold voltage ($V_T = V_{min}$):

$$V_T \approx 2\sqrt{\frac{\gamma\alpha \sin\theta_o}{c}} \qquad (3.14)$$

This final equation confirms that the threshold potential is a consequence of the contact angle hysteresis α. Furthermore, it is possible to reduce this threshold potential by playing on the system parameters such as applying a large Young's angle, a low droplet surface tension or a large capacitance. If this contact angle hysteresis phenomenon was inexistent, then it would be possible to transport a droplet with the smallest of applied voltages (i.e. there would be no set minimum required voltage).

3.2 Design considerations for basic EWOD manipulations

3.2.1 Current EWOD configurations

A wide range of EWOD configuration designs have been developed up to now, notably, as mentioned in the beginning of this chapter, there are two main configuration categories, one of them is the 'open' EWOD configuration [3.29], consisting of a single plate where actuation and ground electrodes are coplanar, in this case the droplet needs to sit on both an actuation electrode and a ground electrode while overlapping the other adjacent electrodes in order for the micro actuation to be successful (Figure 3.6 a)). This system is easier to fabricate and some droplet manipulations such as mixing or purification can be easily performed [3.30]. A variation of this configuration (Figure 3.6 b)) was developed by using a micro catenary as a ground electrode instead of having coplanar actuation and ground electrodes [3.31].

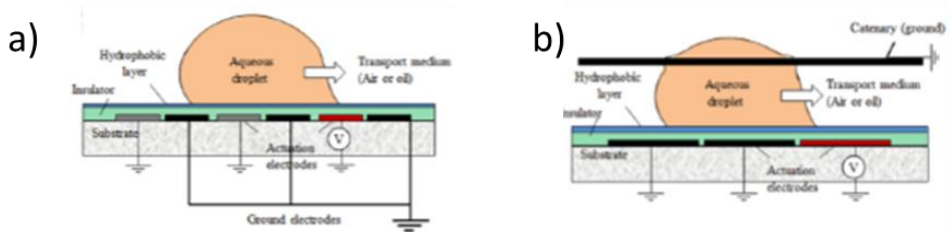

Figure 3.6 : Open EWOD configurations, a) classical coplanar configuration, b) variant using a micro catenary [3.37]

The second main configuration is the 'closed' EWOD configuration [3.32], consisting of a top plate containing the ground electrode and a bottom plate containing the actuations electrodes (Figure 3.7 a)). This configuration requires more fabrication steps than the open system but it enable a large variety of droplet manipulation techniques and also can prevent fast droplet evaporation [3.33]. A variant of this 'closed' system was implemented by Fan et al. who were able to reduce the amount of electrodes by using a cross reference system (Figure 3.7 b)). Indeed, this configuration is composed of multiple electrodes, with variable roles depending on transportation needs (actuation or ground), on the top and bottom plates [3.34].

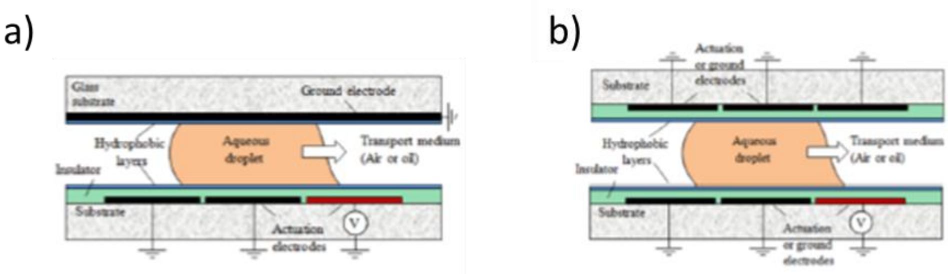

Figure 3.7 : Closed EWOD configurations, a) classical two plate configuration, b) 'cross reference' variant configuration [3.37]

In the case of our research project, we will mainly focus on creating a combination of the open micro catenary, the closed two plates and the cross referencing configurations which will be explained more in details in chapter 4.

3.2.2 Droplet dispensing

In order to create and manipulate various droplets from a common sample, it is necessary to incorporate a droplet dispensing system to the EWOD platform. This droplet dispensing system (in a 'closed' two plate EWOD configuration) is composed of a large electrode, the reservoir, followed by one or two gradually smaller electrodes which serve as intermediaries between the reservoir and the 'active area' (with standard sized electrodes) where droplet manipulations such as mixing, merging, transport, heating and so on take place [3.35]. By designing the reservoir electrode and the intermediary electrode in such a way, the liquid is coerced into gathering in the front part of the reservoir and into overlapping on the first 'active area' electrode. This type of design has been employed for this thesis EWOD platform (Figure 3.8) by using one reservoir electrode and one intermediary electrode :

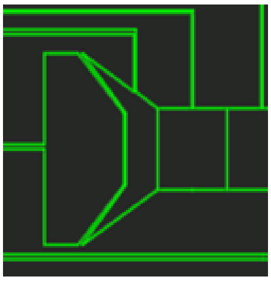

Figure 3.8 : Schematic of two electrode - reservoir design employed in this thesis

A small droplet is formed from the reservoir by the following process : first of all, the reservoir electrode, the intermediary electrode, and a number of adjacent electrodes are activated gradually, thus allowing a liquid chain to be extracted from the reservoir all the way to the last activated electrode (Figure 3.9 a)). Then, when the liquid reaches the final electrode where the droplet is to be formed, all the electrodes between the reservoir electrode and the 'final' electrode are switched off which results in a pinch-off effect of the liquid neck by keeping some of the liquid on the activated 'final' electrode and by forcing the rest to pull back to the activated reservoir electrode (Figure 3.9 b)). Several design parameters influence the success of this dispensing method and the size of the resulting droplet : gap between electrodes, gap between top and bottom plates, reservoir size, electrodes size, and the number of electrodes used for pinch-off among others.

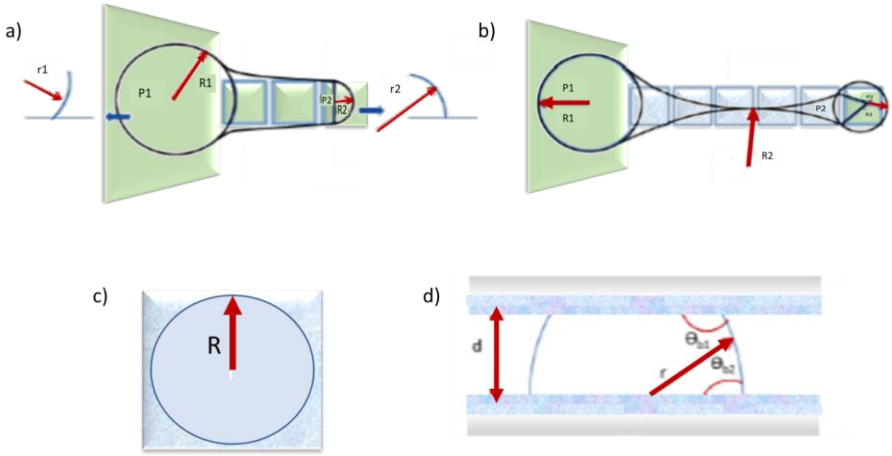

Figure 3.9 : a) liquid neck emerging from the reservoir (reservoir electrode and adjacent electrodes are all on), b) pinch-off effect, c) droplet geometry during electrowetting-based micro actuation (top view), d) droplet geometry during electrowetting-based micro actuation (side view)

The physics behind this dispensing droplet technique was explained [3.36][3.37] by using the Lippmann-Young and the Laplace equations. Indeed, starting from the Laplace equation, the expression of the electrode geometry effects on the pressure inside the liquid is given by:

$$P - P_a = \gamma_{LM}\left(\frac{1}{r} - \frac{1}{R}\right) \qquad (3.15)$$

Where γ_{LM} is the interfacial tension in the liquid-oil medium, R is the principal radius of curvature represented in Figure 3.9 c) and r is the principal radius of curvature described in Figure 3.9 d). Once a liquid neck is starting to emerge from the reservoir, because of the liquid curvature differences between the reservoir and the front of the neck (Figure 3.9 e)), a pressure difference is created. In order for that neck to fully emerge, the electrowetting force resulting from the applied potential has to overcome the previously mentioned pressure difference :

$$P_2 - P_1 = \gamma_{LM}\left(\frac{1}{r_1} - \frac{1}{r_2}\right) - \gamma_{LM}\left(\frac{1}{R_1} - \frac{1}{R_2}\right) = \gamma_{LM}\left(\frac{\cos\theta_{b1} - \cos\theta_{b2}}{d}\right) - \gamma_{LM}\left(\frac{1}{R_1} - \frac{1}{R_2}\right) \quad (3.16)$$

Where d is the gap between the top and bottom plates, θb1 and θb2 are the contact angles respectively for the bottom plate reservoir liquid and for the front liquid neck (Figure 3.9 d)). The relation between the contact angle, the applied voltage and the threshold voltage is given by the following Lippmann-Young equation :

$$\cos\theta(V) - \cos\theta_o = \frac{\varepsilon_o \varepsilon}{2\gamma_{LM} t}(V - V_T)^2 \quad (3.17)$$

Where t refers to the dielectric layer thickness, θ_o and θ are respectively the initial contact angle when the applied voltage V to the dielectric layer is zero and when V is different from zero. By injecting the equation (3.17) into the equation (3.16) with the condition $P_1 > P_2$, the static condition for the liquid neck formation can be deducted :

$$P_1 > P_2 \rightarrow \frac{1}{r_1} - \frac{1}{r_2} = \frac{\varepsilon_0 \varepsilon (V - V_T)^2}{2\gamma_{LM} t d} > \frac{1}{R_2} - \frac{1}{R_1} \quad (3.18)$$

In order to achieve the pinch-off effect (Figure 3.9 b)), the condition $P_2 > P_1$ (i.e. the pressure in the reservoir needs to be smaller than the pressure in the pinch-off area) :

$$P_2 > P_1 \rightarrow \frac{1}{r_2} - \frac{1}{r_1} = \frac{\varepsilon_0 \varepsilon (V - V_T)^2}{2\gamma_{LM} t d} > \frac{1}{R_1} - \frac{1}{R_2} \quad (3.19)$$

Where $R_2 < 0$ at the pinch-off boundary. From this equation (equation (3.19)), it was shown that for a successful pinch-off process, it is better to have a small droplet size and a large aspect ratio [3.36]. Furthermore, by using the number N of electrodes used for the liquid neck expansion and the droplet radius R_3, the magnitude of the curvature radius R_2 can be deducted :

$$|R_2| = \frac{(N^2+1)R_3}{2} \quad (3.20)$$

Thus, by injecting this equation into the previous one :

$$P_2 > P_1 \rightarrow \frac{1}{r_2} - \frac{1}{r_1} = \frac{\varepsilon_0 \varepsilon (V - V_T)^2}{2\gamma_{LM} td} > \frac{1}{R_1} + \frac{2}{(N^2+1)R_3} \qquad (3.21)$$

From this equation, the following general rule was deducted : " As long as the aspect ratio of droplet size/gap is greater than approximately six, only one electrode is required for on-chip droplet dispensing from a reservoir" [3.36][3.37]. Moreover, there are several factors that can help achieve a better control of dispensed droplet volume and droplet dispensing reproducibility. First of all, the nature of the ambient plays a significant role, indeed in the case of an oil ambient, the oil phase hinders the pinch-off process, issue that does occur in the case of an oil medium, thus, an air medium allows a better droplet dispensing reproducibility [3.33]. On the other hand, if the number of pinch-off electrodes is reduced, the amount of liquid volume added by the retracting part of the neck to the formed droplet can be reduced thus the dispensed droplet volume can be controlled [3.35].

3.2.3 Droplet transportation

As mentioned previously (**3.1.2**), by applying an electric potential to adjacent electrodes on which the droplet overlaps, the droplet transport can be induced due to resulting the electrochemical force applied to one side of the droplet (Figure 3.10). Even though both AC and DC voltages can be used for electrowetting-based micro actuation of a droplet, AC voltage is a better candidate due to several reasons : first of all, by using an AC voltage, the contact angle hysteresis effect can be considerably reduced [3.38], the movement of non-aqueous liquids in an air ambient and the movement of solvents in an oil ambient can be facilitated [3.39] [3.40]. But also, the EWOD platform reliability can be increased by reducing the effect of charges trapped in the insulation layer since an alternating electric field is used [3.33].

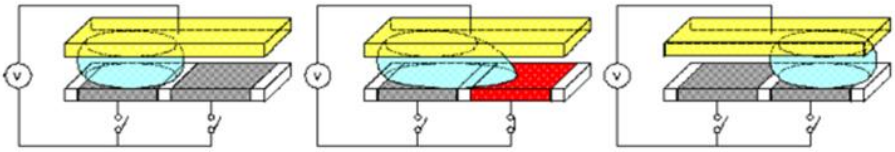

Figure 3.10 : Electrowetting-based micro actuation causing droplet transport [3.58]

One of the critical parameters for droplet transportation is the droplet operations speed. Indeed, the maximum transfer rate directly influences the amount of manipulations that can be performed in a unit time [3.37]. Indeed, in order to produce a device with high throughput, it is necessary to achieve high transportation speeds. It is already established that for the droplet velocity to be independent of the electrode dimensions, the electrode pitch necessarily scales inversely with the droplet transfer rate [3.33]. Up to now, not only is the transport of micro/nano particles such as magnetic beads, and other airborne particles in solution demonstrated [3.41][3.42], but also the transport of non-biological electrolytes, ionic liquids, insulating droplets has been shown [3.40][3.43][3,44].

But in the case of biological applications, the droplet transportation can be hindered notably because some biomolecules tend to absorb on hydrophobic surfaces making the latter permanently hydrophilic which greatly affects the EWOD platform reliability. Therefore, to overcome this issue, several modifications were done to biological protocols and EWOD platform designs : notably, silicon oil was proposed as an ambient [3.45] but some compatibility issues with some organic solvents often used in biological essays might ensue; the use of non-ionic surfactant additives was also proposed as a widely applicable alternative [3.46] [3.47]. But also, design-wise, the addition of “skins” or removable polymer coatings was proposed as a way to renew the EWOD platform surface thus getting rid of the absorbed bodies by easily changing the platform surface after use [3.48].

3.2.4 Droplet merging and splitting

The simplest electrowetting-based droplet micro actuation is droplet merging (Figure 3.11), indeed the merger of two droplets moved towards the same electrode is a natural and instant phenomenon.

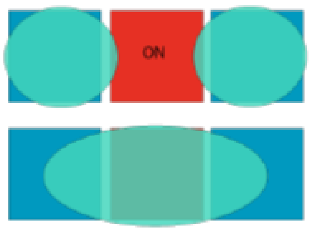

Figure 3.11 : Electrowetting-based droplet merging [3.37]

On the other hand, droplet splitting is a more complex manipulation which was described as followed [3.49]. Firstly, a droplet spread in three switched on electrodes is considered, then the center electrode is switched off resulting in the droplet wetting the remaining uncovered parts of the two opposite electrodes which are still on (Figure 3.12 a)).

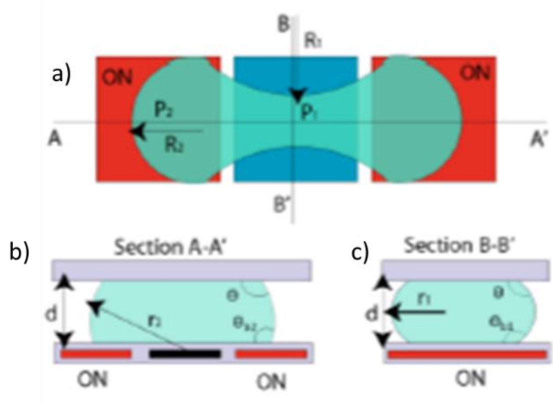

Figure 3.12 : a) Electrowetting-based droplet splitting process (top view), b) cross-section AA’, c) cross-section BB’[3.37]

Thus the radii of curvature r_1 and r_2 increase due to a decrease in the right and left contact angles at three-phase points, resulting in the formation of a neck of radius R_1 which triggers the splitting process. In order to severe that neck, the following condition should be met :

$$\frac{1}{R_1} = \frac{1}{R_2} - \frac{cos\theta_{b2} - cos\theta_{b1}}{d} \quad (3.22)$$

Where d is the gap between the top and bottom plates, the smaller this gap, the easier the splitting process will be. But there is a limit to the gap value above which the splitting process cannot be achieved. In the case of square electrodes of size e, that limit value is given by [3.50] :

$$\frac{d}{e} = -cos\theta_o \quad (3.23)$$

Where , θ_o is the initial contact angle when the applied voltage V is zero.

In order to increase the uniformity of this splitting process, several parameters such as applied voltage, timing, electrode shape can be enhanced [3.51].

3.2.5 Droplet mixing

Electrowetting-based droplet mixing is a critical and complex process when it comes to microscale biological application due to the difficulty to create a mechanically-induced turbulent flow rate. Specially, in the case of EWOD platforms, in order to achieve a high throughput implementation, it is necessary to conduct active mixing processes rather than passive ones which have a low mixing rate (due to extremely low Reynolds number and reduced volume flow rate [3.52]). To create an effective electrowetting-based active mixing process, it is necessary to induce disordered flow patterns inside the droplet.

In the case of an ‘open’ EWOD configuration, high mixing rates (15 ms for 0.5 µL droplets [3.30]) can be achieved by using a single electrode and by inducing self-oscillations inside the droplet (Figure 3.13)[231].

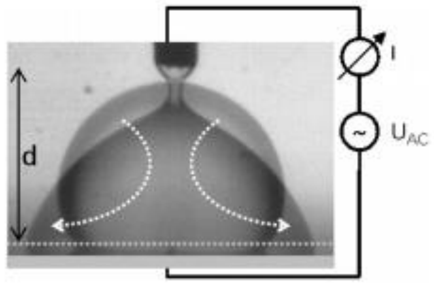

Figure 3.13 : Open EWOD system mixing through induced self-oscillations

[3.57]

In the case of a 'closed' EWOD configuration, the mixing rate greatly depends on the aspect ratio and the smaller the gap between the top and bottom plates (optimum aspect ratio : 0.4 [3.33]). Several active mixing protocols were developed for a 'closed' configuration, among them: a linear translation of the droplet along several electrodes back and forth which achieves a mixing rate slightly higher then that of a passive mixing because of the reversibility effect induced by laminar flow [3.54] even if the mixing time can be increased with an enhanced transport rate and the amount of electrodes used [3.55][3.56]. On the other hand, instead of a linear translation, a continuous loop two-dimensional motion (Figure 3.14) drastically improves the mixing rate (2.8 s for a 1.32µL droplet zig-zagged along a 2x4 electrode array) [3.55][3.56].

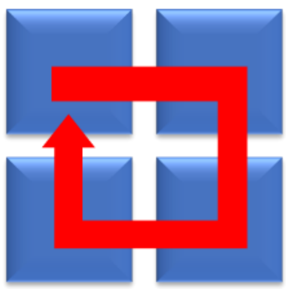

Figure 3.14 : Electrowetting-based mixing through two-dimensional loop motion

3.3 References

[3.1] S. K. Cho, H. Moon and C.-J. Kim, Creating, transporting, cutting, and merging liquid droplets by electrowetting-based actuation for digital microfluidic circuits, Journal of Microelectromechanical Systems, 12 (2003) 70-80.

[3.2] M. G. Pollack, R. B. Fair and A. D. Shenderov, Electrowetting-based actuation of liquid droplets for microfluidic applications, Applied Physics Letters, 77 (2000) 1725-1726.

[3.3] Y. Zhao and S. K. Cho, Microparticle sampling by electrowetting-actuated droplet sweeping, Lab on a Chip, 6 (2006) 137-144.

[3.4] H. Moon, S. K. Cho, R. L. Garrell and C.-J. C. J. Kim, Low voltage electrowetting-on-dielectric, Journal of Applied Physics, 92 (2002) 4080-4087.

[3.5] D. Y. Kim and A. J. Steckl, Electrowetting on Paper for Electronic Paper Display, ACS Applied Materials & Interfaces, 2 (2010) 3318-3323.

[3.6] T. Krupenkin, S. Yang and P. Mach, Tunable Liquid Microlens, Applied Physics Letters, 82 (2003) 316-318.

[3.7] S. C. Jakeway, A. J. de Mello and E. L. Russell, Miniaturized total analysis systems for biological analysis, Fresenius' Journal of Analytical Chemistry, 366 (2000) 525-539.

[3.8] P. Paik, V. K. Pamula and R. B. Fair, Rapid droplet mixers for digital microfluidic systems, Lab on a Chip, 3 (2003) 253-259.

[3.9] Sang Hyun Byun, "Wirelessly powered Electrowetting-On-Dielectric (EWOD)", PhD Thesis (2013)

[3.10] M. G. Lippmann, Relations entre les phénomènes electriques et capillaires, Ann. Chim.Phys., 5 (1875) 494-549.

[3.11] A. R. Wheeler, Putting Electrowetting to Work, Science, 322 (2008) 539-540.

[3.12] B. Berge, Electrocapillarity and wetting of insulator films by water, Comptes Rendus de l'Academie des Sciences Serie II, 317 (1993) 157-163.

[3.13] M. Vallet, B. Berge and L. Vovelle, Electrowetting of water and aqueous solutions on poly(ethylene terephthalate) insulating films, Polymer, 37 (1996) 2465-2470.

[3.14] L. Yeo, and H. C Chang, Electrowetting, Micro/Nanophysics Research Laboratory, Department of Mechanical Engineering, Monash University, (2008) 600-605.

[3.15] F. Mugele and J. Buehrle, Equilibrium drop surface profiles in electric fields, Journal of Physics Condensed Matter, 19 (2007) 375112.

[3.16] T. B. Jones, An electromechanical interpretation of electrowetting, Journal of Micromechanics and Microengineering, 15 (2005) 1184.

[3.17] J. Berthier, Micro and Nano Technologies : Micro-Drops and Digital Microfluidics (2nd Edition), William Andrew, Bighamton, NY, USA, 2012.

[3.18] V. Bahadur and S. V. Garimella, Electrowetting-Based Control of Static Droplet States on Rough Surfaces, Langmuir, 23 (2007) 4918-4924.

[3.19] "Multiscale Dissipative Mechanisms and Hierarchical Surfaces" (Springer Berlin Heidelberg, 2008) p. 153-167.

[3.20] V. Bahadur and S. V. Garimella, Electrowetting-Based Control of Droplet Transition and Morphology on Artificially Microstructured Surfaces, Langmuir, 24 (2008) 8338-8345.

[3.21] N. Cañas, M. Kamperman, B. Völker, E. Kroner, R. M. McMeeking and E. Arzt, Effect of nano- and micro-roughness on adhesion of bioinspired micropatterned surfaces, Acta Biomaterialia, 8 (2012) 282-288.

[3.22] M. G. Pollack, R. B. Fair and A. D. Shenderov, Electrowetting-based actuation of liquid droplets for microfluidic applications, Applied Physics Letters, 77 (2000) 1725-1726.

[3.23] R. Barber and D. Emerson, in "Microdroplet Technology", edited by Day, P., Manz, A. and Zhang, Y., Springer, New York (2012) pp. 77-116.

[3.24] J. Berthier, P. Dubois, P. Clementz, P. Claustre, C. Peponnet and Y. Fouillet, Actuation potentials and capillary forces in electrowetting based microsystems, Sensors and Actuators A: Physical, 134 (2007) 471-479.

[3.25] J. Z. Chen, S. M. Troian, A. A. Darhuber and S. Wagner, Effect of contact angle hysteresis on thermocapillary droplet actuation, Journal of Applied Physics, 97 (2005) 014906-014909.

[3.26] F. Mugele and J.-C. Baret, Electrowetting: from basics to applications, Journal of Physics Condensed Matter, 17 (2005) 705-774.

[3.27] C. W. Extrand and Y. Kumagai, An Experimental Study of Contact Angle Hysteresis, Journal of Colloid and Interface Science, 191 (1997) 378-383.

[3.28] L. Gao and T. J. McCarthy, Contact Angle Hysteresis Explained, Langmuir, 22 (2006) 6234-6237.

[3.29] M. Abdelgawad, S.L.S. Freire, H. Yang, and A.R. Wheeler, All-terrain droplet actuation. Lab on a Chip 8 (2008) 672-677.

[3.30] K.P. Nichols, and H. Gardeniers, A digital microfluidic system for the investigation of pre-steady-state enzyme kinetics using rapid quenching with MALDI-TOF mass spectrometry. Analytical Chemistry 79 (2007) 8699-8704.

[3.31] Y. Fouillet, H. Jeanson, D. Jary, O. Constantin, and C. Vauchier, Moving droplets with microcatenaries, Proceedings of the Seventh International Conference on Miniaturized Chemical and Biochemical Analysis Systems (MicroTAS 2003), Squaw-Valley, CA, 2003, pp. 61.

[3.32] D. Brassard, L. Malic, F. Normandin, M. Tabrizian, and T. Veres, Water-oil core-shell droplets for electrowetting-based digital microfluidic devices. Lab on a Chip 8 (2008) 1342-1349.

[3.33] R.B. Fair, Digital microfluidics: is a true lab-on-a-chip possible? Microfluid Nanofluid 3 (2007) 245-281.

[3.34] S.-K. Fan, C. Hashi, and C.-J. Kim, Manipulation of multiple droplets on NxM grid by cross-reference EWOD driving scheme and pressure-contact packaging, Micro Electro Mechanical Systems, 2003. MEMS-03 Kyoto. IEEE The Sixteenth Annual International Conference on, 2003, pp. 694-697.

[3.35] H. Ren, R.B. Fair, and M.G. Pollack, Automated on-chip droplet dispensing with volume control by electro-wetting actuation and capacitance metering. Sensors and Actuators B 98 (2004) 319-327.

[3.36] H. Ren, Electro-wetting based sample preparartion: an initial study for droplet transportation, creation an on-chip digital dilution, Electrical and computer engineering, Duke University, 2004.

[3.37] L. Malic, "Electrowetting on dielectric digital microfluidic platform with nanostructured biosensor interface for enhanced two-dimensional surface plasmon resonance imaging detection", PhD Thesis (2009)

[3.38] N. Kumari, V. Bahadur, and S.V. Garimella, Electrical actuation of electrically conducting and insulating droplets using ac and dc voltages. Journal of Micromechanics and Microengineering 18 (2008) 105015.

[3.39] D. Chatterjee, B. Hetayothin, A.R. Wheeler, D.J. King, and R.L. Garrell, Droplet-based microfluidics with nonaqueous solvents and solutions. Lab on a Chip 6 (2006) 199-206.

[3.40] M.G. Pollack, Electrowetting-based microactuation of droplets for digital microfluidics, Electrical and computer engineering, Duke University, 2001.

[3.41] G.J. Shah, P.-Y. Chiou, J. Gong, A.T. Ohta, J.B. Chou, M.C. Wu, and C.-J. Kim, Integrating optoelectronic tweezers for individual particle manipulation with digital microfluidics using electrowetting-on-dielectric (EWOD), MEMS 2006, Istanbul, Turkey, 2006, pp. 130.

[3.42] V. Srinivasan, V. Pamula, K.D. Rao, M. Pollack, J.A. Izatt, and R. Fair, 3-D IMAGING OF MOVING DROPLETS FOR MICROFLUIDICS USING OPTICAL COHERENCE TOMOGRAPHY, MicroTAS, 2003.

[3.43] P. Dubois, G. Marchand, Y. Fouillet, J. Berthier, T. Douki, F. Hassine, S. Gmouh, and M. Vaultier, Ionic Liquid Droplet as e-Microreactor. Analytical Chemistry 78 (2006) 4909-4917.

[3.44] N. Kumari, V. Bahadur, and S.V. Garimella, Electrical actuation of dielectric droplets. Journal of Micromechanics and Microengineering 18 (2008) 085018.

[3.45] V. Srinivasan, V.K. Pamula, and R.B. Fair, An integrated digital microfluidic lab-on-a-chip for clinical diagnostics on human physiological fluids. Lab on a Chip 4 (2004) 310-315.

[3.46] O. Raccurt, J. Berthier, P. Clementz, M. Borella, and M. Plissonnier, On the influence of surfactants in electrowetting systems. Journal of Micromechanics and Microengineering 17 (2007) 2217-2223.

[3.47] V.N. Luk, G.C. Mo, and A.R. Wheeler, Pluronic additives: a solution to sticky problems in digital microfluidics. Langmuir : the ACS journal of surfaces and colloids 24 (2008) 6382-6389.

[3.48] H. Yang, V.N. Luk, M. Abeigawad, I. Barbulovic-Nad, and A.R. Wheeer, A World-to-Chip Interface for Digital Microfluidics. Analytical Chemistry 81 (2009) 1061-1067.

[3.49] S.-K. Cho, H. Moon, J. Fowler, and C.-J. Kim, Splitting a liquid droplet for electrowetting-based microfluidics., In: Proceedings of 2001 ASME Inter Mech Eng Congress and Expo, New York, NY, 2001.

[3.50] J. Berthier, Microdrops and Digital Microfluidics, William Andrew Publishing, 2008.

[3.51] H. Ren, V. Srinivasan, and R.B. Fair, Design and testing of an interpolating mixing architecture for electrowetting-based droplet-on-chip chemical dilution, TRANSDUCERS, Solid-State Sensors, Actuators and Microsystems, 12th International Conference on, 2003, 2003, pp. 619-622 vol.1.

[3.52] R.B. Fair, Digital microfluidics: is a true lab-on-a-chip possible? Microfluid Nanofluid 3 (2007) 245-281.

[3.53] F. Mugele, J.C. Baret, and D. Steinhauser, Microfluidic mixing through electrowetting-induced droplet oscillations. Applied Physics Letters 88 (2006) 204106.

[3.54] H.-W. Lu, F. Bottausci, J.D. Fowler, A.L. Bertozzi, C. Meinhart, and C.-J.C.J. Kim, A study of EWOD-driven droplets by PIV investigation. Lab on a Chip 8 (2008) 456-461.

[3.55] P. Paik, V.K. Pamula, and R.B. Fair, Rapid droplet mixers for digital microfluidic systems. Lab on a Chip 3 (2003) 253-259.

[3.56] P. Paik, V.K. Pamula, M.G. Pollack, and R.B. Fair, Electrowetting-based droplet mixers for microfluidic systems. Lab on a Chip 3 (2003) 28-33.

[3.57] F. Mugele, Microfluidic mixing through electrowetting-induced droplet oscillations. Appl. Phys. Lett. 88, 204106 (2006).

[3.58] http://www.vandamlab.org/knowledge/microfluidics

[3.59] http://www.ramehart.com/newsletters/2008-09_news.htm

Chapter 4. Design and Fabrication of an EWOD-based SELEX platform

4.1 Overall system description

This chapter will give a detailed presentation of the device designed and fabricated for this research project. As mentioned in chapter 2, several microfluidic platforms have been created for SELEX process implementation, but all those platform could carry only some steps of the SELEX process notably the separation step or the amplification step. But also, these platforms are flow-through-based thus necessitating a significant amount of reactant.

Our platform on the other hand, is an EWOD-based digital microfluidic platform designed to automatically carry out the whole SELEX process without any user intervention needed. First of all, it is necessary to break down the different steps of this SELEX process in order to explain more in detail how will our platform carry them out automatically.

A mentioned in chapter three, the SELEX process (Figure 4.1) is composed mainly of five steps for DNA or RNA aptamer generation. Even though this platform is designed to generate both DNA and RNA aptamers, for the sake of explanation, we will consider the case of RNA aptamer generation. After a preliminary denaturation, a random RNA library is first ‘incubated’ in a micro-liter droplet with the target for the selection process to take place resulting in two categories of oligonucleotides : the ones that formed a aptamer-target complex and the unbound oligonucleotides. For this step, two integrated heater/thermal sensor systems will be used alongside the basic EWOD electrodes.

Then comes the following step which is the separation between the unbound sequences and the aptamer-target complexes. Up to now, when it comes to microfluidic implementations of the SELEX process, this step is mainly carried out using magnetic micro-beads coated with the target, therefore, after binding, those beads conjugated with the whole aptamer-target complexes are ‘trapped’ using a magnetic field and the unbound sequences flow through the waste channel. For this thesis, the separation step will be handled differently, by applying the principle of electrophoretic mobility used for CE-SELEX [2.18], the Cassie/Wenzel wetting transition phenomenon and the electrowetting-based splitting process in order to conduct the whole separation process in one droplet. Thus a novel design of micro range electrode arrays will be used for this step.

After separation comes the elution step where, after discarding the unbound sequences, the aptamer-target sequences are eluted before proceeding with the selected oligonucleotides amplification. For this step, we opted for a thermal-based elution, thus the previously introduced heater/thermal sensor system will also be used.

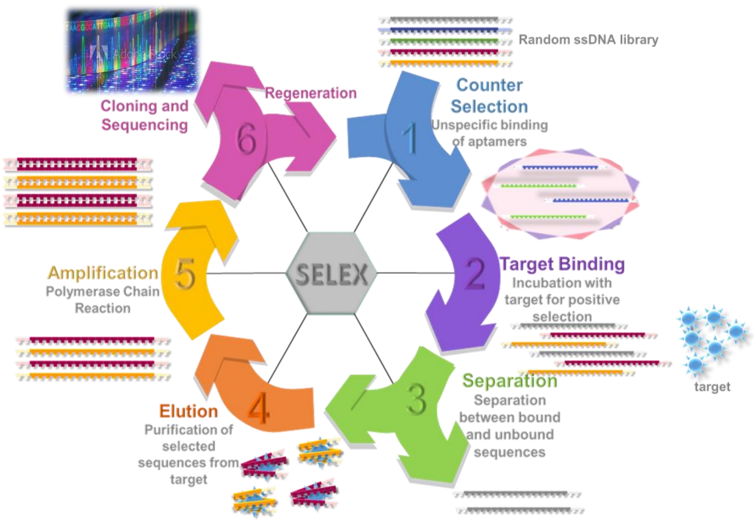

Figure 4.1 : Schematic representation of the SELEX process

Then comes the amplification step for which, the NASBA process will be used. NASBA or Self-Sustained Sequence Replication (3SR) is a sensitive, isothermal transcription-based amplification process. Not only is its isothermal nature an advantage for simple heating system integration without the need of a special thermocycling system, but also the amplification and detection (if necessary) is not time consuming : an HIV-1 NASBA and detection time of 90 minutes for up to 48 samples was demonstrated [4.1]. Figure 4.2 shows the activities that take place during a NASBA process: following the selected RNA sequences denaturation, an initiation phase takes place where a specific forward primer is hybridized to the RNA, followed by an extension of the primer while the RNA is degraded (using RNase H) in order to achieve the hybridization of a specific primer to the cDNA. That primer is then extended to form a double-stranded T7 promoter sequence which will be used by the T7 DdRp to produce many RNA copies to our targeted RNA. Then comes the amplification cyclic phase during which the reverse primer hybridizes with the formed RNA which will be degraded during the extension process; then the cDNA will bind to the forward primer to enable that cDNA extension while using the forward primer as a template. This results in the formation of a double stranded T7 promoter and, using the T7 DdRp, a new RNA copy will be produced at each cycle.

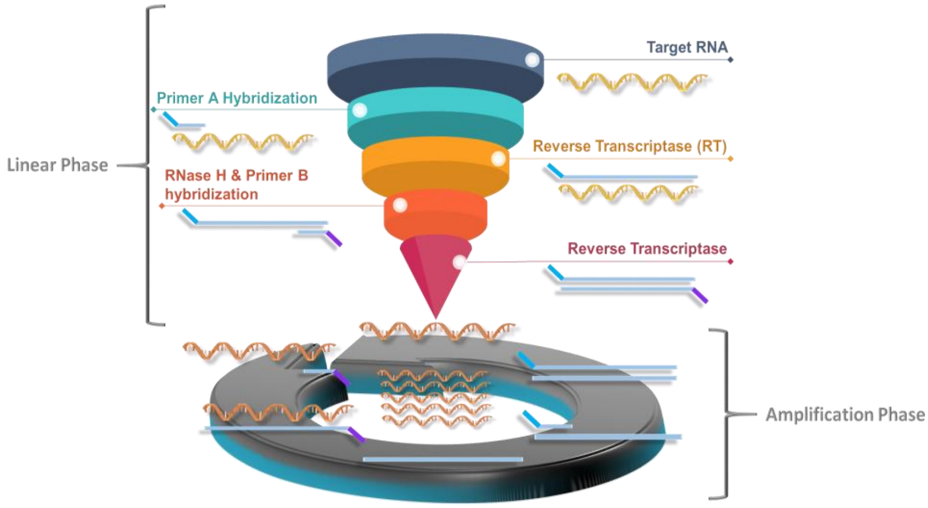

Figure 4.2 : A schematic of the NASBA process

Even though the chemistry behind the NASBA process is quite complex, it is a natural process that requires only a trigger. Indeed, a primer 'mix' containing all the components required for this NASBA (except the enzymes) is mixed with the aptamer, after hybridization, the enzymes are added and a self-sustained amplification is carried on at 41ºC. Depending on the user's preferences, it is possible to carry on a real-time monitoring of this amplification process by adding to the mixture molecular beacons [4.2] (Figure 4.3) allowing both amplification and detection to take place simultaneously. Those molecular beacons are DNA oligonucleotides containing a quencher at their 3' end and a fluorophore at their 5' end. Since the two ends have complementary sequences, the molecular beacon adopts a hairpin configuration which allows the quencher to absorb the fluorophore light. The hairpin loop sequence being complementary with amplified RNA sequence, the molecular beacon binds to that RNA which induce the quencher-fluorophore 'complex' separation thus the light emitted by the fluorophore increases in intensity and can be detected [4.1].

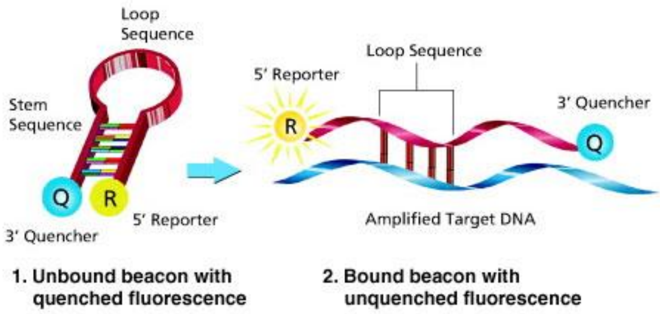

Figure 4.3 : Molecular beacons working principle (Sigma-Aldrich)

The different characteristics of NASBA are presented in the following table:

- A single step isothermal amplification reaction at 41°C.
- Especially suited for RNA analytes because of the integration of RT into the amplification process.
- The single-stranded RNA product is an ideal target for detection by various methods including solution probe hybridization.
- The fidelity of NASBA is comparable to that of other amplification processes using DNA polymerases lacking the 3' exonuclease activity.
- The use of a single temperature eliminates the need for special thermocycling equipment.
- Efficient ongoing process resulting in exponential kinetics caused by production of multiple RNA copies by transcription from a given cDNA product.
- Unlike amplification processes, such as PCR in which the initial primer level limits the maximum yield of product, the amount of RNA product obtained in NASBA exceeds the level of primers by at least one order of magnitude.
- NASBA RNA product can be sequenced directly with a dideoxy method using RT and a labeled oligonucleotide primer.
- The intermediate cDNA product can be made double-stranded, ligated into plasmids, and cloned.
- Three enzymes are required to be active at the same reaction conditions.
- Low temperature can increase the nonspecific interactions of the primers. However, these interactions are minimized by the inclusion of DMSO.
- A single melting step is required to allow annealing of the primers to the target.
- The NASBA enzymes are not thermostable and thus can only be added after the melting step.
- The primers are not incorporated in the amplicon and thus labeled primers can not be used for detection.
- The length of the target sequence to be amplified efficiently is limited to approx 100 to 250 nucleotides.

Table 4.1 : Characteristics of NASBA [4.1]

For this amplification step, a mixing electrode and a heating/thermal sensing system are integrated to our EWOD platform.

Following this amplification, the droplet is directed to either an outlet for sequencing and characterization or it is directed to the following SELEX round operating line.

Based on this above detailed SELEX process, we developed an EWOD platform (Figure 4.4) with two operating lines each corresponding to a SELEX round and in between them, transition electrodes and two different outlets (Figure 4.4 a)) are added in order not only to automatically move from one round to the other, but also to give the user the freedom to decide up to how much rounds will the sample be directed to an outlet for sequencing and characterization.

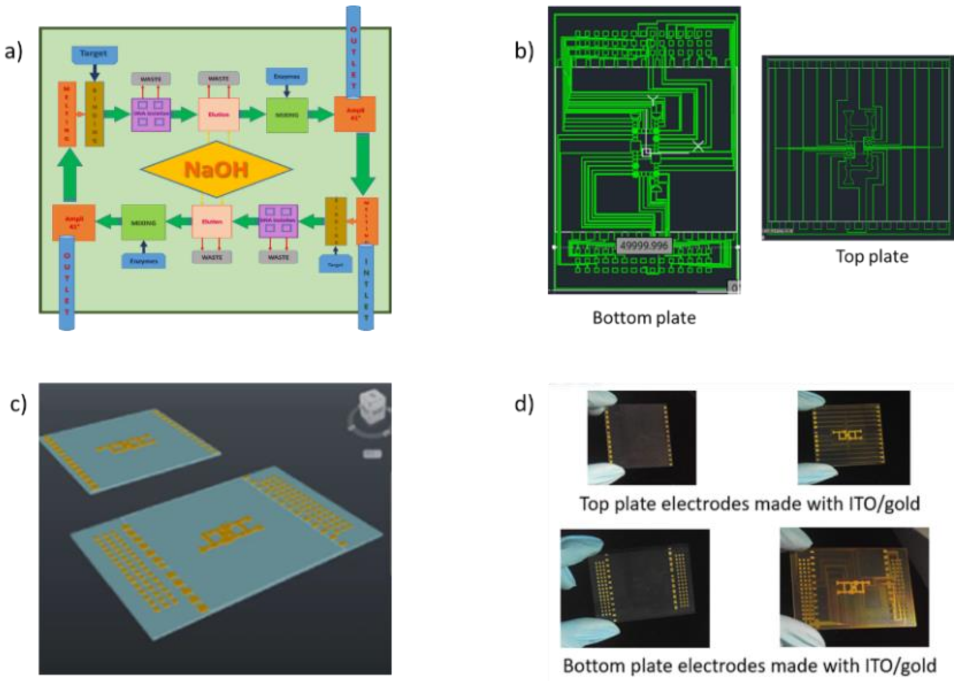

Figure 4.4 : EWOD-based SELEX platform, a) schematic layout, b) Fabrication photo-mask design, c) 3D modelling, d) picture of the fabricated platform

4.2 Originality

The EWOD-based SELEX platform developed in this thesis (Figure 4.5) is based on various novel concepts, from fabrication methods to biological protocols reconfiguration.

First of all, up to now the whole SELEX process has not been implemented on an EWOD platform which allows to contain the whole aptamer generation reactions in a single µL range droplet thus saving a significant amount of reactants. Moreover, by using a completely automatic system, the user can launch a chain of droplets moving on the different parts of this platform one after another, that way, it is possible to run a large number of SELEX processes simultaneously.

But also, specially for the separation part, a new protocol based on a new exploitation of several principles combined such as the Cassie/Wenzel wetting/de-wetting transitions, the electrophoretic mobility properties of oligonucleotides, and vertical electrowetting-based droplet splitting, therefore avoiding the use of any foreign body which will require throughout washing thus reactants loss.

In order to guaranty a good progress of the SELEX process or any other biological essay, heat generation and temperature control play a significant role, therefore, in the phase 1 characterization of our platform we focused on the conception of a highly sensitive integrated RTD transparent heater/ thermal sensor system which operates with a low threshold voltage using a novel material double doping protocol.

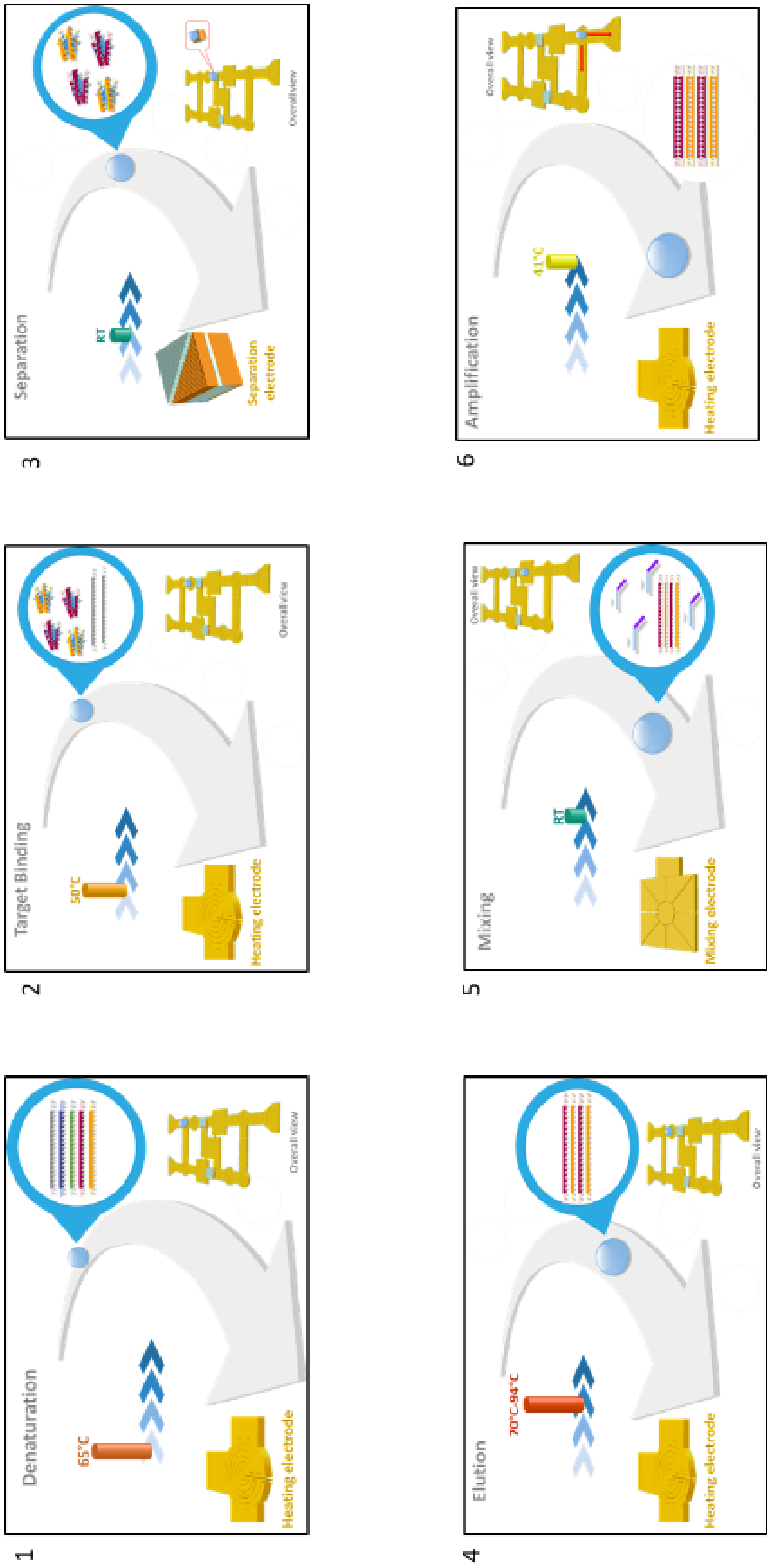

Figure 4.5 : EWOD-based SELEX platform reactional stages

4.3 Specific design considerations and fabrication steps

Our device design, the fabrication steps and the principles used are detailed in this part.

4.3.1 Basic EWOD parts

In between the several ‘specialized’ electrodes of our platform, are basic EWOD actuation electrodes fabricated through deposition and patterning soft lithography clean room processes.

4.3.1.1. Overall Design

The overall platform was fabricated on a glass substrate using transparent materials to allow an easy future integration of optical detection or control systems. Indeed, ITO was used as the conductive material for actuation. When it comes to the dielectric layer, it is necessary to optimize the dielectric material to reduce the device failure rates due to dielectric layer breakdown. For our device fabrication, we settled for SU8 which acts not only as a dielectric, but also as a hydrophobic layer [4.3], therefore there is no need to have additional fabrication steps for a hydrophobic layer deposition.

Moreover, due to a limitation in the number of electrodes that can be used for the automation system integration, it was essential to combine different ‘closed’ EWOD. As mentioned in chapter 3, during the recent years, several EWOD configurations have been developed (Figure 3.7), thus we used for our system (Figure 4.6), a ‘cross-referencing’ configuration with a large common ground electrode on the top plate and a micro catenary.

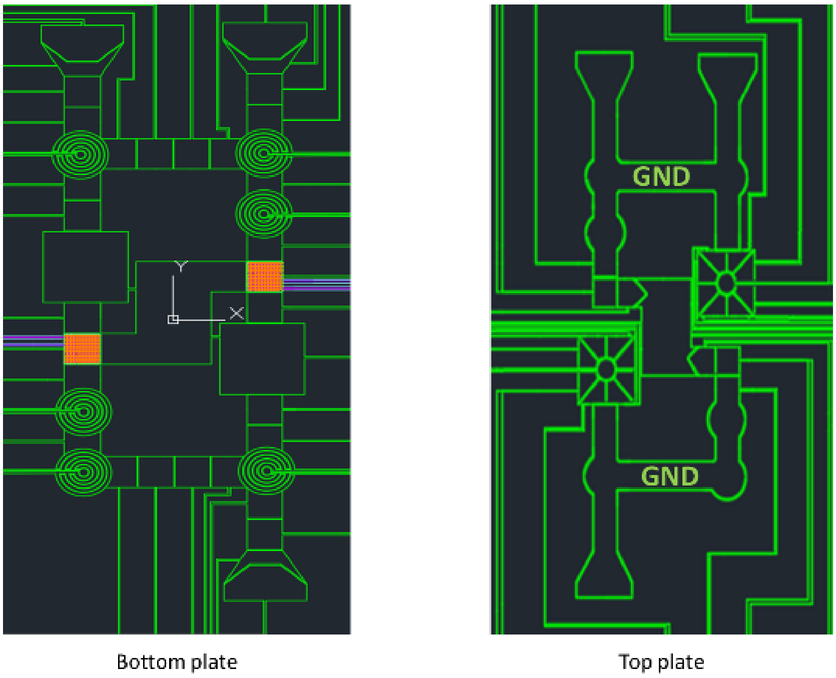

Figure 4.6 : EWOD-based SELEX platform combined ‘closed’ EWOD configuration

4.3.1.2. Mixing electrodes design

As mentioned in chapter 3, several mixing methods have been developed up to now, even though the laws of mixing inside a droplet are yet to be well defined in a theoretical point of view [4.4][4.5], according to empirical results, in order to achieve a high throughput system, the most efficient mixing method is attained by creating a chaotic flow inside the droplet. Thus we have designed a mixing system composed of several electrodes that a programmed to induce the droplet rotation on its main axis using the vortex principle (Figure 4.7). The center electrode is always turned on whiles the peripheric electrodes are switched on / off following a rotation pattern . The electrodes used for this mixing system are fabricated through the same protocol than basic EWOD actuation electrodes.

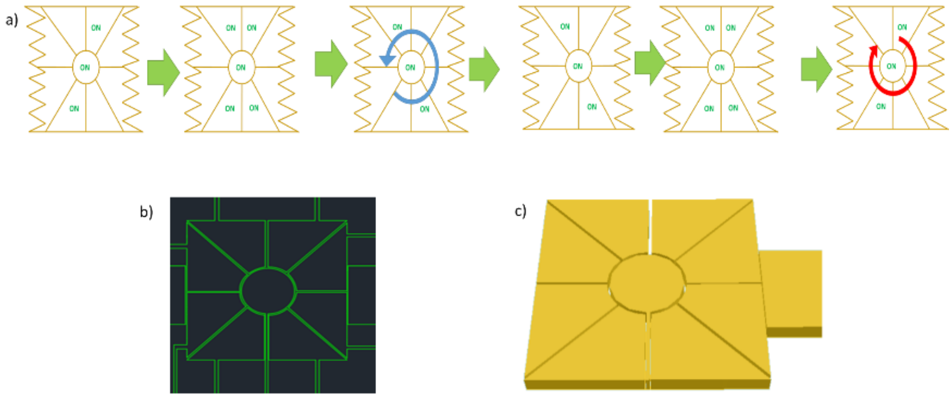

Figure 4.7 : EWOD mixing system, a) working principle, b) photo mask design, c) 3D model

4.3.1.3. Heading/thermal sensing system design

The micro heaters and RTD integrated to our platform can create a uniform heating and a fast thermal response while minimizing the power needed to operate the whole system [4.6].

Due to the crucial role that heating plays in a vast majority of biological essays such as PCR, NASBA, cell culture among others, several microfluidic heating implementations have been developed such as Peltier-based [4.8], lasers [4.9], hot plates [4.10], incubators [4.11] external heating systems. But also, integrated heating systems using resistive heaters [4.12], microwaves [4.13], or again micro-Peltier devices [4.14].

In the case of this EWOD platform, since conductive electrodes are already patterned for electrowetting-based droplet micro actuation, it is more straightforward to use that conductive material to also pattern the heating/ thermal sensing system alongside the EWOD electrodes. Several heating options can be implemented in a 'closed' EWOD configuration such as microwave dielectric heating, dielectrophoresis Joule heating or resistive Joule heating.

Microwave dielectric heating is achieved by inducing dissipation of the energy associated with the alignment of induced and intrinsic dipole moments due to the applied high frequency electric fields [4.15]. On the other hand, when a current resulting from applied high frequency electric fields circulates through a droplet, the triggered dielectrophoresis phenomenon can induce heat dissipation [4.16]. But, since these two methods are dependent on the chemical composition of the liquid involved and since the integration of a thermal control and feedback system is difficult, it is necessary to look for another heating option.

For an easier integration for an EWOD platform, a resistive heater and RTD system seems to be an excellent candidate [4.17]. Indeed, not only is the temperature linearly proportional to the resistance [4.17], but also, the same electrode can be used for both heating and RTD feedback control [4.18]. Indeed, with this method, heating/RTD and electrowetting-based actuation can be controlled separately using the same electrode by altering the electrical bias levels [4.19]. This alternation between actuation and heating (Figure 4.8) is achieve through the following operation: in order to move, an electrical potential is applied between the top ground electrode and the bottom actuation electrodes (Figure 4.8 a)) and for heating, the potential is applied through the single bottom plate resistive heating electrode thus rendering it biased (Figure 4.8 b)).

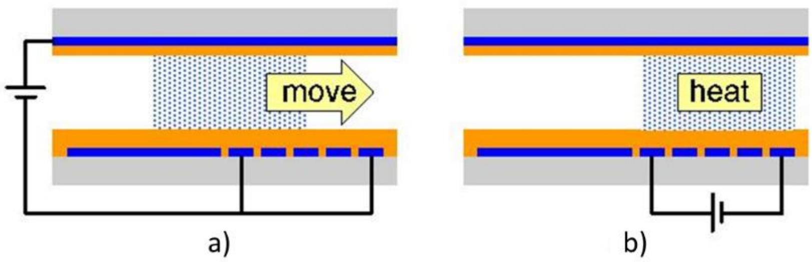

Figure 4.8 : Electrowetting-based actuation and heating/thermal sensing alternation principle, a) Movement, b)Resistive heating [4.18]

ITO is also an excellent conductive material candidate since it allows a more sensitive RTD feedback [4.20] through a higher thermal coefficient of resistance, and it does not degrade through heating like other metals such as copper. Gold was used as an overall interconnection material due to its high conductivity and its resistance to oxidation [4.19].

4.3.1.4. Fabrication

The fabrication was carried on in a MEMS clean room at the Seoul National University Inter-university Semiconductor Research Center.

Several microfabrication processes were used for this fabrication (Figure 4.9) : photolithography, wet etching, evaporation and lift-off.

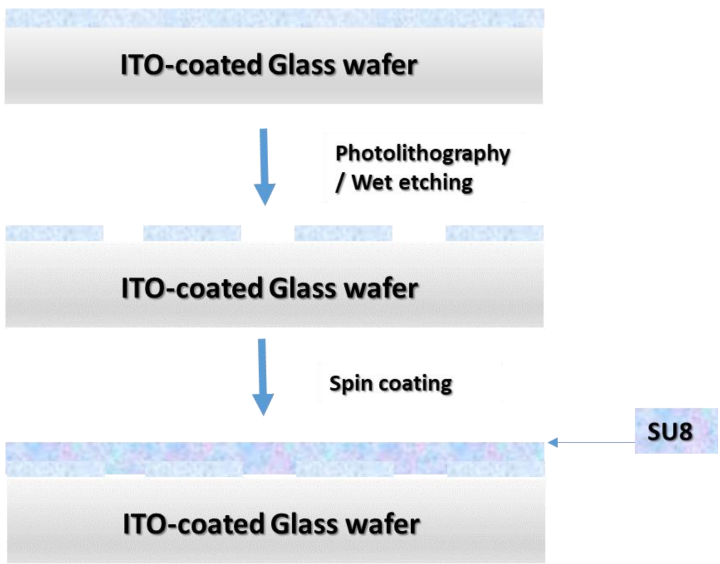

Figure 4.9 : Process flow of basic EWOD parts fabrication

First of all, a 200nm ITO coated glass wafer was first cleaned using acetone and isopropyl alcohol combined with ultrasonication steps. After blow drying with a nitrogen gas gun, the wafer was dehydrated on a hot plate. In order to carry on with the ITO electrodes patterning, photolithography (Figure 4.10) was first carried on to remove some parts of a Photoresist (PR) in order to create an etching mask. That mentioned PR (AZ1512) is first spin coated on the previously cleaned and dehydrated ITO coated glass wafer, then after the pre exposure baking steps, our previously designed photo mask (Figure 4.11) is used for exposure with the Aligner MA6: the PR is selectively exposed via a UV light passing through the transparent parts of the photo mask, which modifies the chemical properties of the PR. Then, after post exposure bake, the exposed PR was developed revealing the desired pattern. Then the wafer was again baked before wet etching in order to avoid affecting the PR etching mask during the etching process. After wet etching, the PR etching mask was removed using a PR stripper solution.

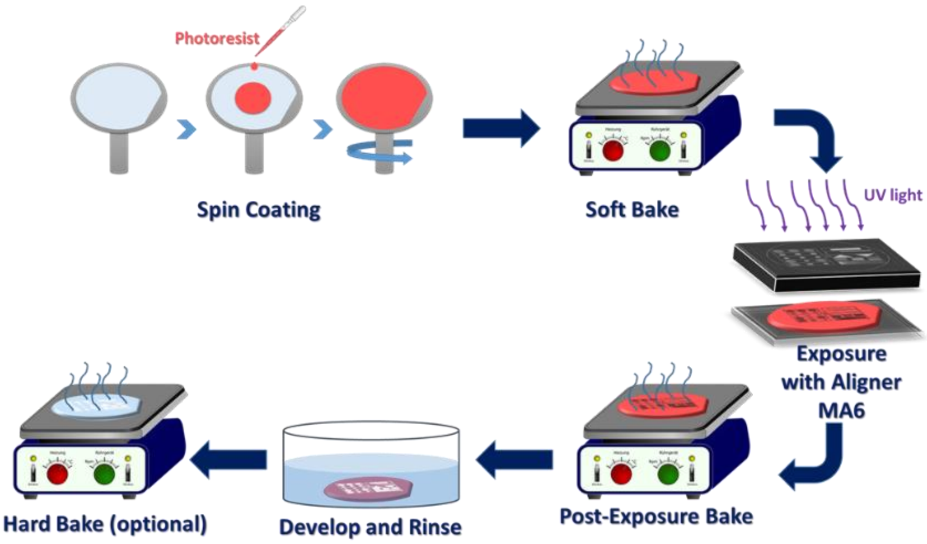

Figure 4.10 : Photolithography working principle

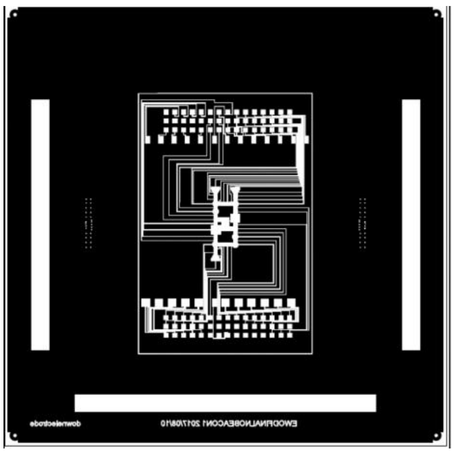

Figure 4.11 : Photo mask used for electrodes patterning

The gold interconnections (Figure 4.12) were patterned through lift-off process (Figure 4.13) : before metal deposition, a combination of Lift-Off Resist and PR were coated and patterned followed by E-gun evaporation of chrome and gold, afterwards lift-off is carried on through sonication in an acetone solution resulting in the metal interconnections patterning.

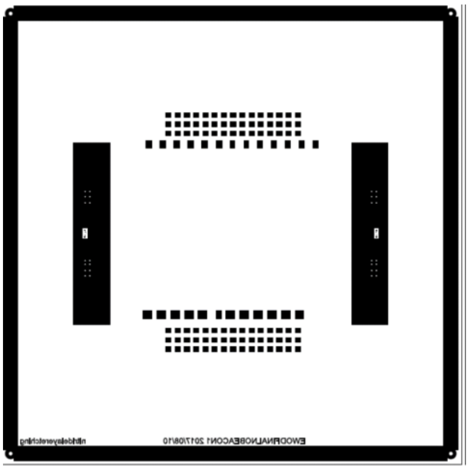

Figure 4.12 : Photo mask used for gold interconnections patterning

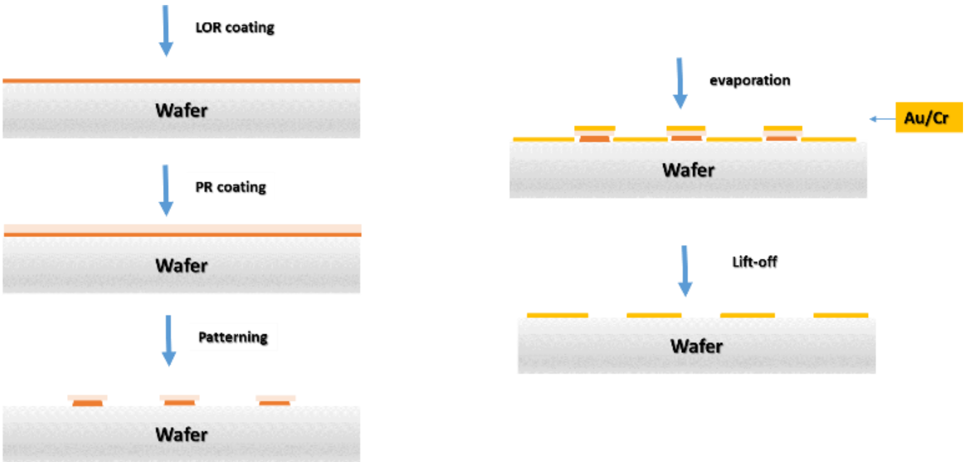

Figure 4.13 : Lift-off process working principle

As mentioned before, SU8 was used as a dielectric and a hydrophobic layer also using photo lithography.

4.3.2 Separation parts

The second critical part, alongside the heater/thermal sensor system, is the aptamer-target complexes and unbound sequences separation step. Indeed, up to now, since no bead-less separation method inside a droplet has been developed, an EWOD-based implementation of the whole SELEX process in one platform was still not developed. This following sub-sections will define more in details how this novel separation method works and the different principles used.

4.3.2.1 Cassie-Wenzel wetting/de-wetting transition

As defined in chapter 3, the Cassie [4.22] and Wenzel [4.23] wetting states are the two extreme of static wettability on textured surfaces (such as superhydrophobic surfaces) describing respectively the non-wetting state and the complete wetting state [4.21] which present different surface energies [4.24].

Superhydrophobic surfaces have emerged as a valuable tool for LOC, heat transfer or energy systems applications. A superhydrophobic surface is, like a lotus leaf, a surface on which a droplet can roll down easily with a slight tilt [4.25]. By studying the surface of that lotus leaf, it was possible to artificially produce superhydrophobic surfaces by creating a dual roughness [4.26-4.43]. On those surfaces, electrowetting was used to induce the Cassie/Wenzel transition [4.44] by reducing the solid-liquid interfacial energy with the applied electric potential. This induced transition was achieved not only for micro structured surfaces [4.45][4.46][4.47], but also for nano structured surfaces [4.48][4.49][4.50][4.51]. As a result, the following observation came to light : there is no complete and spontaneous reversibility of this Cassie/Wenzel wetting transition, when the applied voltage is turned off, mainly due to an energy barrier (Figure 4.14) for the de-wetting or reverse transition [4.47][4.48].

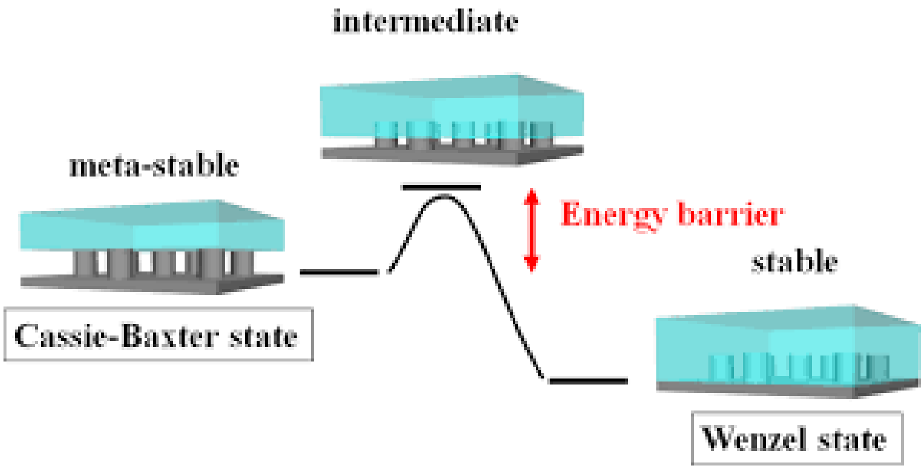

Figure 4.14 : Irreversible Cassie/Wenzel wetting transition due to Energy barrier [4.52]

Different attempts were made to induce the de-wetting transition over the years, even if that reverse transition was successfully achieved, the methods disadvantages outweighed the achievements.

On one hand, reversibility was achieved by using an oil ambient to reduce the dissipative forces and to promote competitive wetting [4.50]; but also, electrolysis was used to generate a gas layer leading to the Cassie/Wenzel de-wetting transition [4.53]. But these two methods are not applicable for biological applications.

On the other hand, reversible wetting transitions were observed through current pulse application to vaporize a layer of liquid [4.48] but this method is associated with significant mass loss which is not desirable for our application.

However, Kumari et al [4.21] used a three-electrode electrowetting-based system to induce Cassie/Wenzel wetting and de-wetting transitions without sample loss and without complex additions to the basic superhydrophobic design. In this setup (Figures 4.15, 4.16), a two plates 'closed' EWOD configuration with a micro catenary is used to form the three-electrode combination : that micro catenary is used as the ground electrode while either the top or the bottom plate can be used to apply the electric potential between the targeted electrode and the droplet. The droplet is initially in Cassie state (Figure 4.16 a)), when an electric potential is applied between the superhydrophobic bottom plate electrode and the droplet, the droplet transitioned into Wenzel state (Figure 4.16 b)) and kept that state even after the potential is removed (Figure 4.16 c)). The reverse wetting transition is triggered by applying an electric potential between the top plate electrode and the droplet (Figure 4.16 d)) and finally, the droplet deposited gently onto the superhydrophobic bottom plate when that previously applied potential is turned off (Figure 4.16 e)). This method was proved to be repetitive, thus reliable.

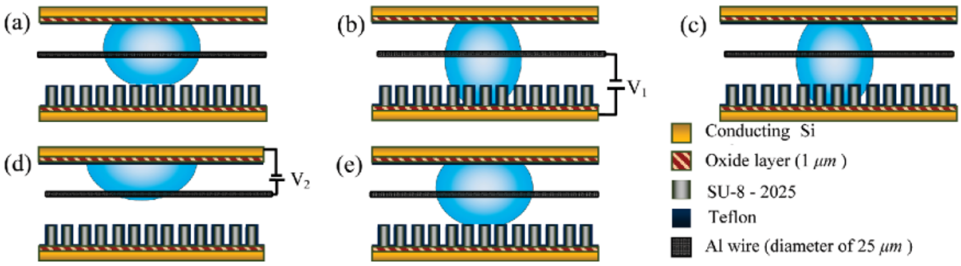

Figure 4.15 : Electrowetting induced Cassie/Wenzel wetting and de-wetting transitions working principle, a)initial spontaneous Cassie state on bottom superhydrophobic plate, b) Wenzel state induced through bottom plate actuation, c) droplet remaining in Wenzel state when bottom plate potential turned off, d) reverse transition triggered by actuating top plate, e) droplet gently resting on bottom plate when top plate actuation stopped [4.21]

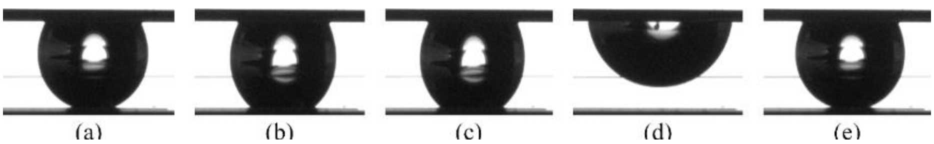

Figure 4.16 : Electrowetting induced Cassie/Wenzel wetting and de-wetting transitions experimental visual feedback [4.21]

As mentioned previously, CE-SELEX was developed around the electrophoretic mobility changes induced during the binding process between the oligonucleotides and the targets. Binding with a target triggers an electrophoretic mobility change of the aptamer-target complex, which modifies the migration time of that complex compared to the non-binding oligonucleotide (Figure 4.17)[4.54]. Unbound sequences co-migrate in a single band while aptamer-target complexes migrate either faster or slower depending on whether the target increases or decreases the complex mobility.

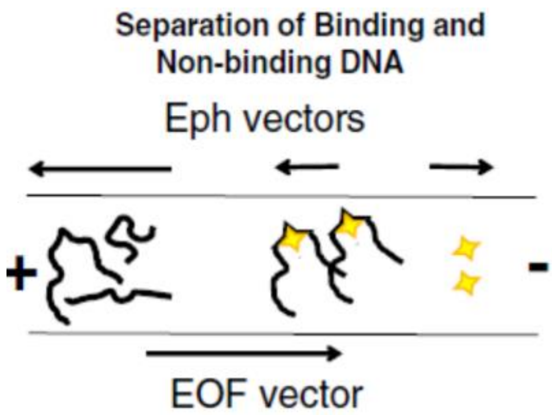

Figure 4.17 : Electrophoretic mobility shift induced by target binding [4.54]

By combining this electrophoretic mobility change phenomenon and the Cassie/Wenzel wetting and de-wetting transitions, it is possible to perform the aptamer-target complexes/unbound sequences separation inside a droplet.

4.3.2.2 Design

Using the above mentioned phenomenon, an EWOD-based separation method was designed. That separation happens when the droplet transition to Wenzel state is achieved and the potential is removed (Figure 4.15 c)) : at that stage the selective migration of aptamer-target complexes (Figure 4.17) is induced by integrating vertical electrodes to the micropillars used to achieve a superhydrophobic surface (Figure 4.15).

After the migration is induced, the droplet is vertically split between a daughter droplet containing the aptamer-target complexes and a daughter droplet containing the unbound sequences (Figure 4.18).

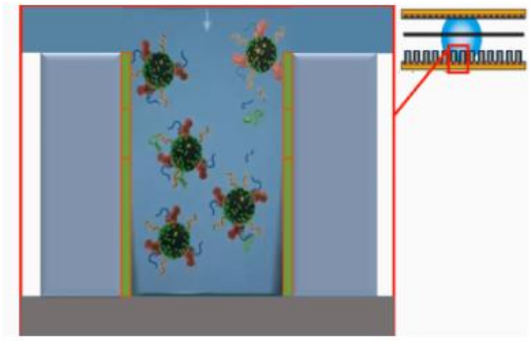

Figure 4.18 : Vertical electrodes integration to micropillars

As mentioned previously, the binding can slow down or increase the complex mobility, and the developed separation method can easily adapt to those variations with the versality of EWOD actuation (Figure 4.19).

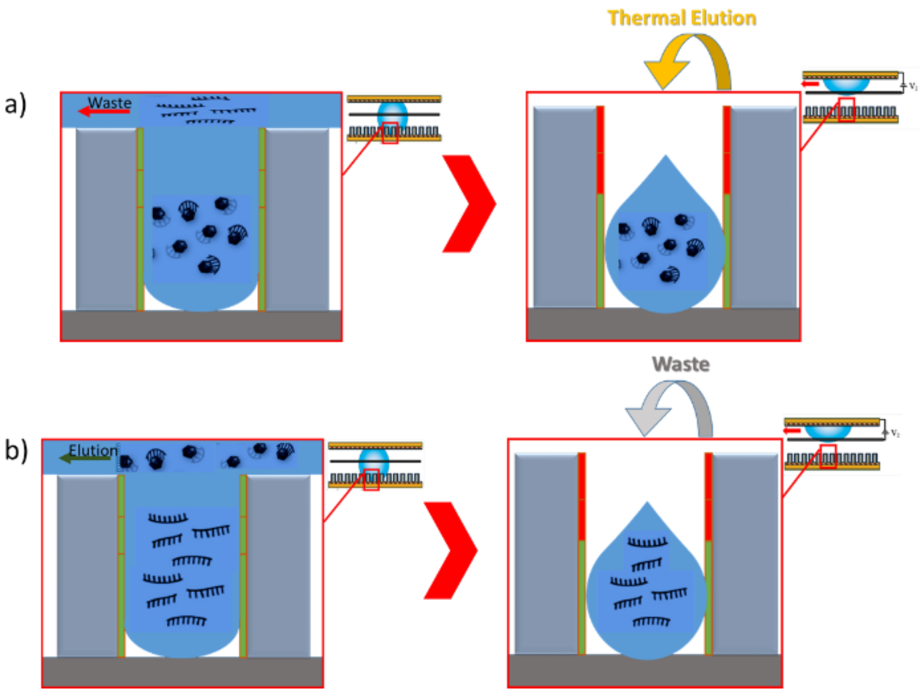

Figure 4.19 : Protocol adaptation to Electrophoretic mobility shifts cases, a) when the migration speed is increased, b) when the migration speed is decreased

Furthermore, to fabricate the superhydrophobic surface used for the wetting transitions, SU8 micropillars were designed in order to ensure that the droplet will be in Cassie state initially and will transition to Wenzel state when an electric potential is applied.

4.3.2.3 Fabrication

Following the previous fabrication steps, in order to fabricate (Figure 4.20) the two vertical electrodes on top of the basic EWOD actuation electrode, a combination of patterning through lift-off, using a photo mask (Figure 4.21), followed by electroplating growth and dielectric deposition, repeated twice (Figure 4.22). Then micro wells (Figure 4.23) are patterned to form the final microstructure for the superhydrophobic effect.

Figure 4.20 : Vertical electrodes fabrication process flow

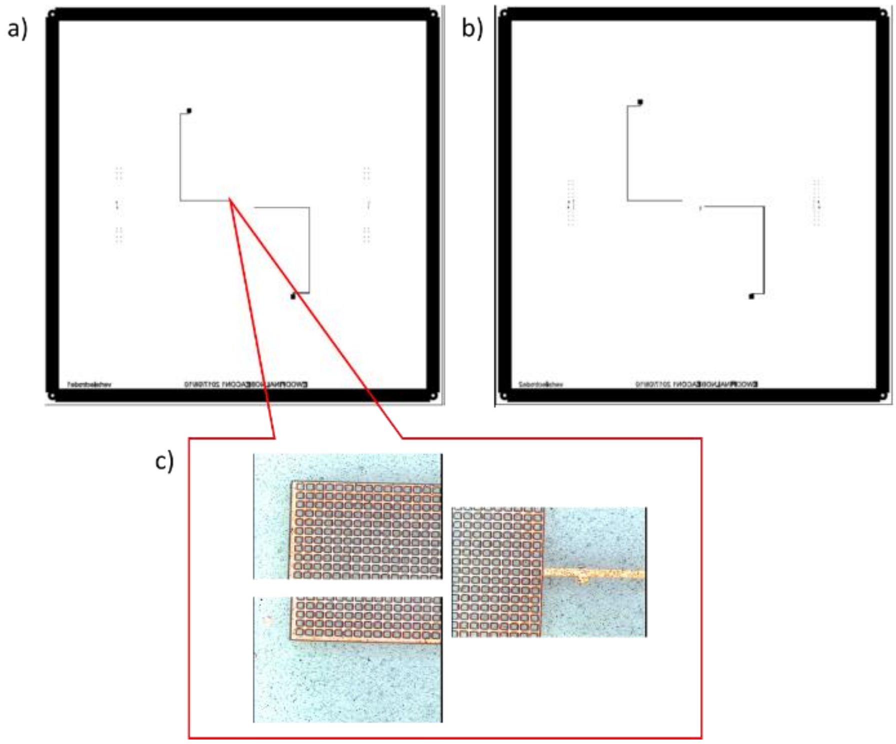

Figure 4.21 : Vertical electrode arrays photo masks, a) vertical electrode 1, b) vertical electrode 2, c) fabrication visual result

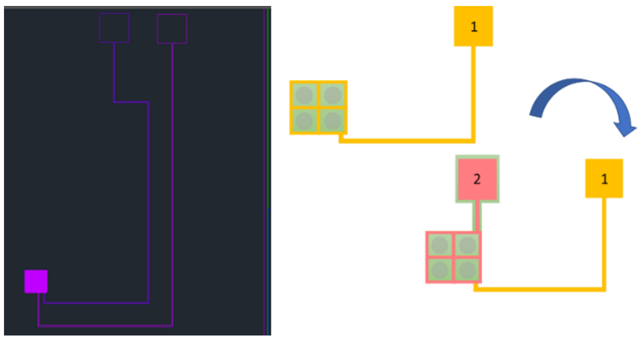

Figure 4.22 : Vertical electrodes schematic fabrication (top view)

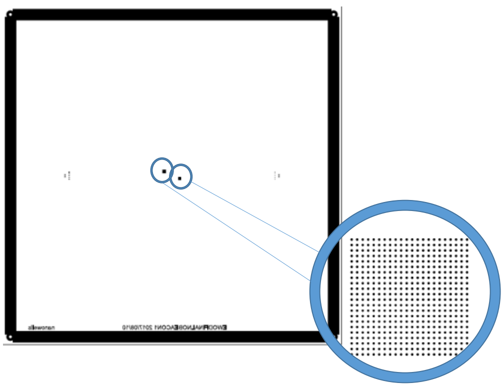

Figure 4.23 : Micro wells photo mask

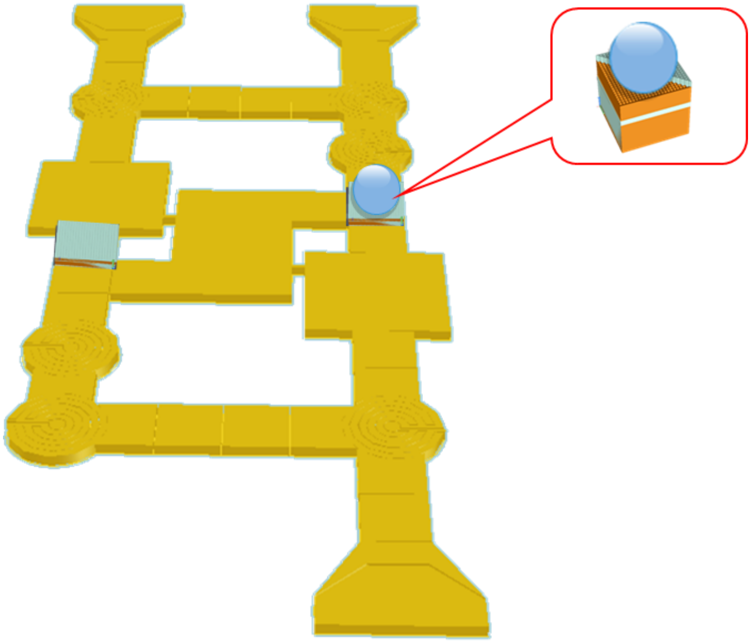

Figure 4.24 : 3D model of the whole vertical electrodes system

4.4 References

[4 .1] Deiman, B., van Aarle, P. & Sillekens, P. Mol Biotechnol (2002) 20: 163.

[4.2] Tyagi, S. and Kramer, F. R. (1996) Molecular beacons: probes that fluoresce upon hybridization. *Nature Biotech.* **14**, 303–308.

[4.3] Vijay Kumar and N. N. Sharma, “SU-8 as Hydrophobic and Dielectric Thin Film in Electrowetting-on-Dielectric Based Microfluidics Device,” Journal of Nanotechnology, vol. 2012, Article ID 312784, 6 pages, 2012.

[4.4] J. Berthier, Microdrops and Digital Microfluidics, William Andrew Publishing, 2008.

[4.5] H.-W. Lu, F. Bottausci, J.D. Fowler, A.L. Bertozzi, C. Meinhart, and C.-J.C.J. Kim, A study of EWOD-driven droplets by PIV investigation. Lab on a Chip 8 (2008) 456-461.

[4.6] Chen, L., Manz, A., Day, P. J. R., *Lab Chip* 2007, **7**, 1413–1423.

[4.7] Chen Supin, “Production of positron emission tomography (PET) radiotracers with electrowetting-on-dielectric (EWOD) digital microfluidics”, PhD Thesis (2014)

[4.8] G. Maltezos, M. Johnston, K. Taganov, C. Srichantaratsamee, J. Gormon, D. Baltimore, W. Chantratita and A. Scherer, "Exploring the limits of ultrafast polymerase chain reaction using liquid for thermal heat exchange: A proof of principle," Applied Physics Letters, vol. 97, p. 264101, 2010.

[4.9] M. N. Slyadnev, Y. Tanaka, M. Tokeshi and T. Kitamori, "Photothermal temperature control of a chemical reaction on a microchip using an infrared diode laser," Analytical Chemistry, vol. 73, pp. 4037-4044, 2001.

[4.10] K. Domansky, W. Inman, J. Serdy, A. Dash, M. H. M. Lim and L. G. Griffith, "Perfused Multiwell plate for 3D liver tissue engineering," Lab on a Chip, vol. 10, pp. 51-58, 2010.

[4.11] W. Ren, J. Perumal, J. Wang, H. Wang, S. Sharma and D.-P. Kim, "Whole ceramic-like microreactors from inorganic polymers for high temperature or/and high pressure chemical syntheses," Lab on a Chip, 2014, 14, 779-786, vol. 14, pp. 779-786, 2014.

[4.12] Y.-H. Chang, G.-B. Lee, F.-C. Huang, Y.-Y. Chen and J.-L. Lin, "Integrated polymerase chain reaction chips utilizing digital microfluidics," Biomedical Microdevices, vol. 8, pp. 215-225, 2006.

[4.13] A. J. L. Morgan, J. Naylon, S. Gooding, C. John, O. Squires, J. Lees, D. A. Barrow and A.Porch, "Efficient microwave heating of microfluidic systems," Sensors and Actuators B: Chemical, vol. 181, pp. 904-909, 2013.

[4.14] G. Maltezos, M. Johnston and A. Scherer, "Thermal management in microfluidics using micro-Peltier junctions," Applied Physics Letters, vol. 87, p. 154105, 2005.

[4.15] D. Issadore, K. J. Humphry, K. A. Brown, L. Sandberg, D. A. Weitz and R. M. Westervelt, "Microwave dielectric heating of drops in microfluidic devices," Lab on a Chip, vol. 9, pp. 1701-1706, 2009.

[4.16] T. B. Jones, "Liquid dielectrophoresis on the microscale," Journal of Electrostatics, Vols. 51-52, pp. 290-299, 2001.

[4.17] J.-H. Wei, W.-S. Hsu and S.-K. Fan, "Realizing temperature-controlled digital microfluidic chips with versatile microelectrodes," in 2nd IEEE International Conference on Nano/Micro Engineered and Molecular Systems, Bangkok, Thailand, pp.981-984, 2007.

[4.18] W. Nelson, I. Peng, J. A. Loo, R. L. Garrell and C.-J. Kim, "An EWOD droplet microfluidic chip with integrated local temperature control for multiplex proteomics," in Proceedings of IEEE International Conference on Micro Electro Mechanical Systems, Sorrento, Italy, pp. 280-283, 2009.

[4.19] W. Nelson, I. Peng, J. A. Loo, R. L. Garrell and C. J. Kim, "An EWOD Droplet Microfluidic Chip with Integrated Local Temperature Control for Multiplex Proteomics," *2009 IEEE 22nd International Conference on Micro Electro Mechanical Systems*, Sorrento, 2009, pp. 280-283.

[4.20] Y. V. Deshmukh, Industrial heating: principles, techniques, materials, applications, and design, New York: CRC Press, 2005.

[4.21] Electrowetting-Induced Dewetting Transitions on Superhydrophobic Surfaces**,** Niru Kumari and Suresh V. Garimella**,** *Langmuir* 2011 *27* (17), 10342-10346**.**

[4.22] Cassie, A. B. D. *Discuss. Faraday Soc.* 1948, 3, 11– 15.

[4.23] Wenzel, T. N. *J. Phys. Colloid Chem.* 1949, 3, 1466– 1467.

[4.24] He, B.; Patankar, N. A.; Lee, J. *Langmuir* 2003, 19, 4999– 5003.

[4.25] Y. Kwon *et al*., "Development of micro variable optics array," *2014 IEEE 27th International Conference on Micro Electro Mechanical Systems (MEMS)*, San Francisco, CA, 2014, pp. 72-75.

[4.26] A. Lafuma and D. Quere, "Superhydrophobic States," Nature Materials, Vol. 2, No. 7, 2003, pp. 457-460.

[4.27] Multiscale Roughness and Stability of Superhydrophobic Biomimetic Interfaces, Michael Nosonovsky, *Langmuir* 2007 *23* (6), 3157-3161

[4.28] Wetting and Wetting Transitions on Copper-Based Super-Hydrophobic Surfaces, N. J. Shirtcliffe,*, G. McHale,M. I. Newton, and, and C. C. Perry**,** *Langmuir* 2005 *21* (3), 937-943.

[4.29] Design and Fabrication of Micro-textures for Inducing a Superhydrophobic Behavior on Hydrophilic Materials**,** Liangliang Cao, Hsin-Hua Hu, and, and Di Gao**,** *Langmuir* 2007 *23* (8), 4310-4314.

[4.30] Mimicking the Lotus Effect: Influence of Double Roughness Structures and Slender Pillars, Neelesh A. Patankar, *Langmuir* 2004 *20* (19), 8209-8213.

[4.31] Superhydrophobic Surfaces : from Natural to Artificial, L. Feng *et al*, *Adv Mater* 2002 *14*.

[4.32] Roughness-induced non-wetting, S. Herminghaus, *Europhysics Letters* 2000 *52*.

[4.33] Superhydrophobicity Due to the Hierarchical Scale Roughness of PDMS Surfaces, B. Cortese *et al*, *Langmuir* 2008 *24*.

[4.34] Fabrication of micro/nano integrated roughened structure using nanosphere lithography (NSL), A. L. Thangawng, and J. Lee, *ASME International Mechanical Engineering Congress. Proceedings of IMECE04, Anaheim* 2004.

[4.35] Nanoengineered multiscale hierarchical structures with tailored wetting properties, H. E. Jeong *et al*, *Langmuir* 2006 *22*.

[4.36] Hierarchical Silicon Etched Structures for Controlled Hydrophobicity/Superhydrophobicity, Y. Xiu *et al*, *Nano Lett* 2007 *7*.

[4.37] Artificial lotus leaf by nanocasting, M. Sun *et al*, *Langmuir* 2005 *21*.

[4.38] One-step solution-immersion process for the fabrication of stable bionic superhydrophobic surfaces, S. Wang, L. Feng, and L. Jiang, *Adv Mater* 2006 *18*.

[4.39] Dual-scale Roughness Produces Unusually Water-Repellent Surfaces, N. J. Shirtcliffe *et al*, *Adv Matter* 2004 *16*.

[4.40] A Nonlithographic Top-Down Electrochemical Approach for Creating Hierarchical (Micro-Nano) Superhydrophobic Silicon Surfaces, M. F. Wang, N. Raghunathan, and B. Ziaie, *Langmuir* 2007 *23*.

[4.41] Effects of Rugged Nanoprotusions on the Surface Hydrophobicity and Water Adhesion of Anisotropic Micropatterns, X. Gao, X. Yao, and L. Jiang, *Langmuir* 2007 *23*.

[4.42] Wetting Properties of the Multiscaled Nanostructured Polymer and Metallic Superhydrophobic Surfaces, E. Bormashenko *et al*, *Langmuir* 2006 *22*.

[4.43] Large Slip of Aqueous Liquid Flow over a Nanoengineered Superhydrophobic Surface, C. H. Choi, and C. J. Kim, *Phys Rev Lett* 2006 *96*.

[4.44] Mugele, F.; Baret, J. C. *J. Phys.: Condens. Matter* 2005, 17, R705– R774.

[4.45] Herberston, D. L.; Evans, C. R.; Shirtcliffe, N. J; McHale, G.; Newton, M. I. *Sens. Actuators, A* 2006, 130, 189– 193.

[4.46] Bahadur, V.; Garimella, S. V. *Langmuir* 2007, 23, 4918– 4924.

[4.47] Bahadur, V.; Garimella, S. V. *Langmuir* 2008, 24, 8338– 8345.

[4.48] Krupenkin, T. N.; Taylor, J. A.; Wang, E. N.; Kolodner, P.; Hodes, M.; Salamon, T. R. *Langmuir* 2007, 23, 9128– 9133.

[4.49] Wang, Z.; Ci, L.; Chen, L.; Nayak, S.; Ajayan, P. M.; Koratkar, N. *Nano Lett.* 2007, 7, 697– 702.

[4.50] Dhindsa, M.; Smith, N. R.; Heikenfeld, J.; Rack, P. D.; Fowlkes, J. D.; Doktycz, M. J.; Melechko, A. V.; Simpson, M. L. *Langmuir* 2006, 22, 9030– 9034.

[4.51] Verplanck, N.; Galopin, E.; Camart, J.-C.; Thomy, V.; Coffinier, Y.; Boukherroub, R. *Nano Lett.* 2007, 7, 813– 817.

[4.52] Wetting Transition from the Cassie–Baxter State to the Wenzel State on Textured Polymer Surfaces**,** Daiki Murakami, Hiroshi Jinnai, and Atsushi Takahara, *Langmuir* 2014 *30* (8), 2061-2067.

[4.53] Lee, C.; Kim, C.-J. *Phys. Rev. Lett.* 2011, 106, 014502.

[4.54] Durney BC, Crihfield CL, Holland LA. Capillary electrophoresis applied to DNA: determining and harnessing sequence and structure to advance bioanalyses (2009–2014). *Analytical and Bioanalytical Chemistry*. 2015;407:6923-6938.

Chapter 5. Platform automation and Phase 1 Characterization

5.1 Automation with DropBot system

The fabricated platform was directly actuated, without any packaging, using the DropBot DMF automation system developed by the Wheeler Lab [5.1].

Through this system, it is possible to induce electrowetting-based micro actuation of droplets. Up to 120 independent channels can be driven, and it is possible to measure in real-time the droplet position, velocity, and the electrostatic driving force, which enable, regardless of the DMF platform used, a more accurate control of the electrowetting-based biological essays protocols. It is also possible to maintain precise and uniform actuation forces by using a real-time tuning of applied potentials [5.2].

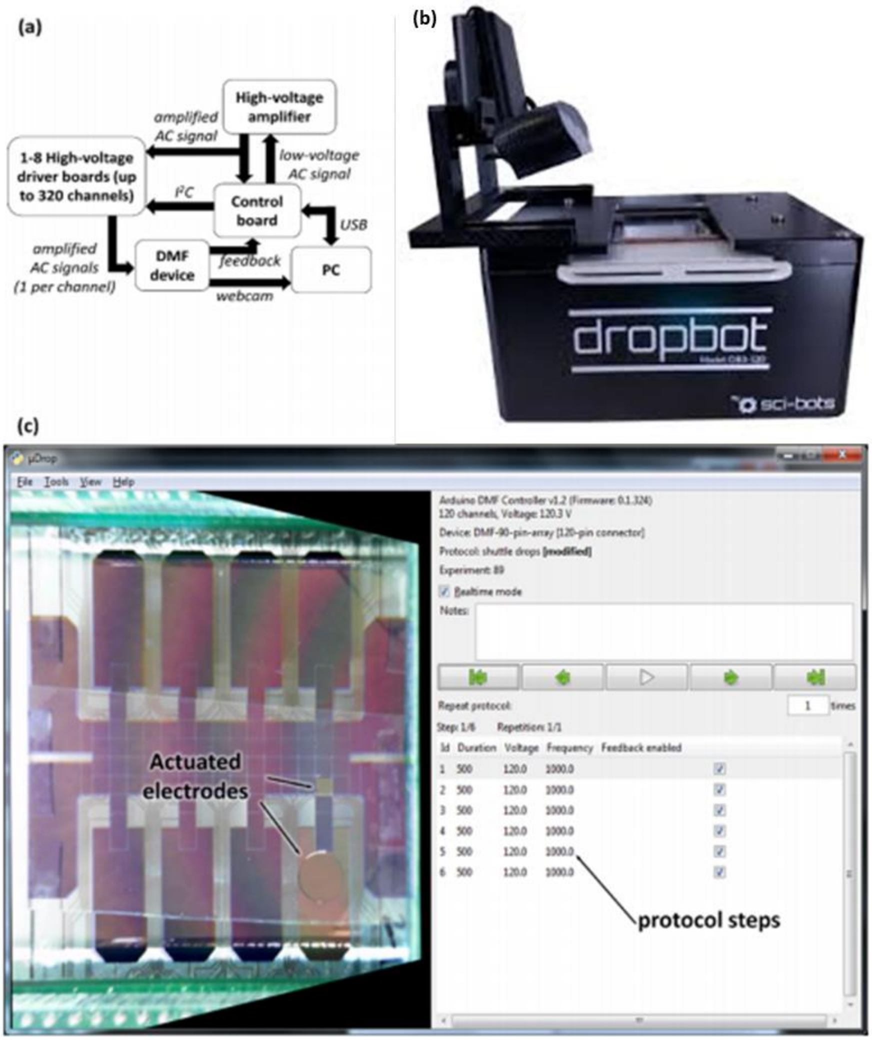

Figure 5.1 : DropBot DMF automation system, a) Working block diagram, b) Photograph of the DropBot system, c) Screenshot of the affiliated software [5.1]

Actuation can be done through an interactive interface (Figure 5.1 c)) on which the user can mouse-click on the real-time visual feedback overlay to actuate a given electrode.

With this system, it is possible to enter the whole SELEX protocol designed for our EWOD platform and automatically run that protocol using a closed-loop controlled system.

5.2 Heater and sensor calibration

As mentioned in chapter 4, the resistive heating electrodes principle was used for our EWOD-based SELEX platform heater/thermal sensor system. After fabrication, it is necessary to run calibration protocols to assess the RTD response to temperature changes in order to determine the heater actuation input necessary and the sensor performance.

5.2.1 Calibration

The heater/thermal sensor system is calibrated using the bath type experiment. Through that calibration technique, it is possible to compute the temperature coefficient of resistance (TCR) and the sensitivity of the heater/thermal sensor system [5.3]. This bath type calibration technique give a linear variation of resistance in function of temperature, which depends on various parameters such as : the purity of the conductive material, the uniformity of the actuating layer among others. With the bath type calibration setup, a gradual step variation of temperature is applied, using a laboratory hot plate (Fisher Scientific ISOTEMP) with constant stirring to reduce the time needed to reach a steady state temperature and uniformity, and the corresponding changes in resistance were obtained using an LCR meter since the heater/thermal sensor system is passive thus necessitates a constant current input (about 10mA) (Figure 5.2). A beaker is also used, containing the EWOD platform and K type and J type thermocouples to measure the bath temperature. Those thermocouples are placed in different location to get a uniform assessment of the bath steady temperature in order to achieve an accurate calibration monitoring[5.4].

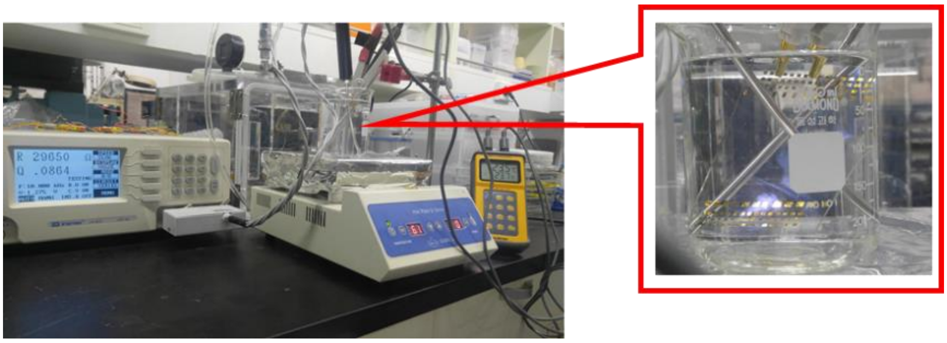

Figure 5.2 : Bath type calibration experimental setup

5.2.2 Results

Using the previously described calibration method, it was possible to determine the heater calibration curves (Figures 5.3,5.4),the sensor response (Figure 5.5), the TCR (Figure 5.6), the normalized response (Figure 5.7) and the sensitivity (Figure 5.8) of our thermal system.

The relationship between temperature and measured resistance is generally defined by :

$$R_T = R_O(1 + \alpha_T * \Delta T) \qquad (5.1)$$

$$\Delta T = T - T_O \qquad (5.2)$$

where R_O and R_T are, respectively, the resistances of an RTD at the initial temperature T_O and at a temperature T; α_T represent the average resistance/temperature relationship of the RTD known as TCR; ΔT is defined as the variation in a temperature relative to the initial temperature. That TCR is given by :

$$\alpha_T = \frac{R_T - R_O}{R_O(\Delta T)} \qquad (5.3)$$

For more precision, these values can be defined with the Callendar-Van Dusen equation to give a general behavior [5.5][5.6] :

$$\frac{R}{Ro} = 1 + \alpha\left[T - \delta\left[\frac{T}{100} - 1\right]\left[\frac{T}{100}\right] - \beta\left[\frac{T}{100} - 1\right]\left[\frac{T}{100}\right]^3\right] \quad (5.4)$$

Where α is the above described constant which characterizes the normalized slope in the 0ºC - 100ºC range, δ is the Callendar constant (Equation (5.5)) which defines the disparity between the actual temperature T_H and the temperature calculated using the linear formula (Equation (5.2)), β is the Van Dusen constant (Equation (5.6)) which serves for the conversion of negative temperatures based on the disparity between the actual temperature T_L and the temperature calculated using only α and δ. These two constants are described by [5.7] :

$$\delta = \frac{T_H - \frac{R*T_H - Ro}{Ro*\alpha}}{\frac{T_H - 1}{100} \text{ x } \frac{T_H}{100}} \qquad (5.5)$$

$$\beta = \frac{T_L - \frac{R*T_L - Ro}{Ro*\alpha} + \delta*\left[\frac{T_L}{100} - 1\right]*\frac{T_L}{100}}{\left[\frac{T_L - 1}{100} \text{ x } \frac{T_L}{100}\right]^3} \qquad (5.6)$$

The quadratic version of Equation (5.4) is used for a more accurate calibration of the heater/thermal sensor system used in this thesis :

$$R_T = R_O\,(1 + AT + BT^2) \qquad (5.7)$$

Where A and B are two constants defined by the following [5.5] :

$$A = \alpha\left[1 + \frac{\delta}{100}\right] \quad (5.8)$$

$$B = -\frac{\alpha\delta}{100^2} \quad (5.9)$$

The obtained experimental curves are as follows :

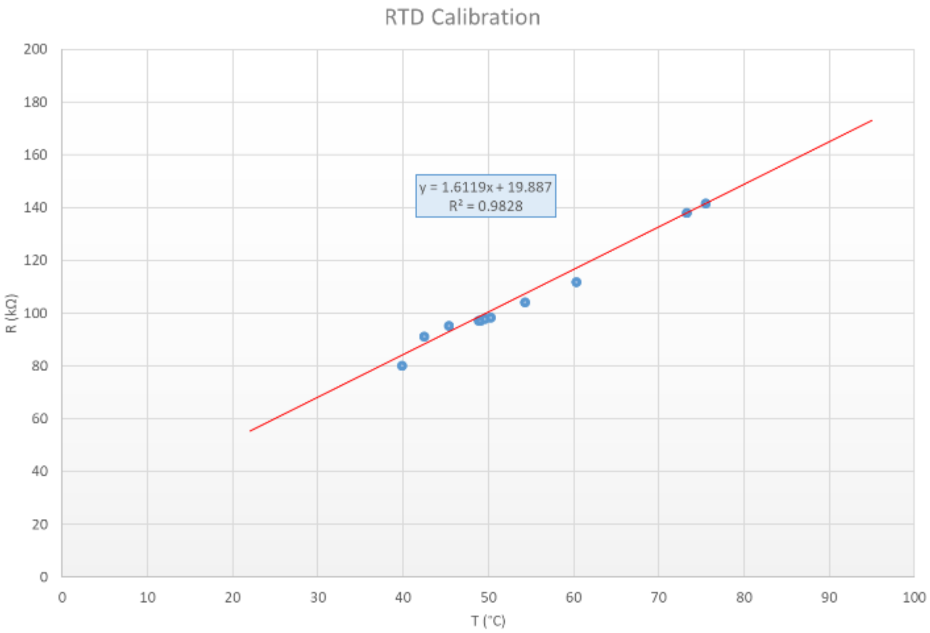

Figure 5.3 : ITO Heater linear calibration

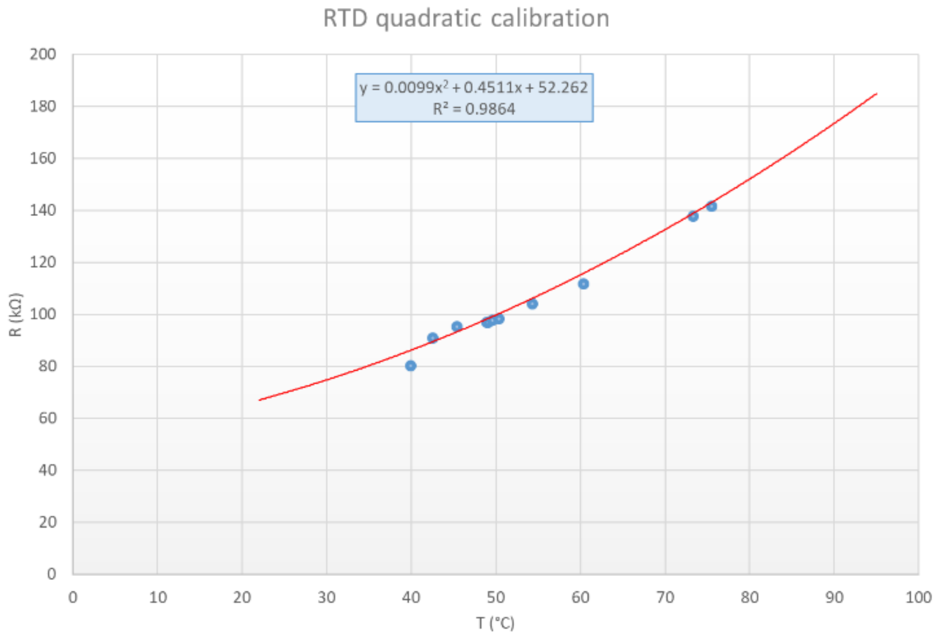

Figure 5.4 : ITO Heater quadratic calibration

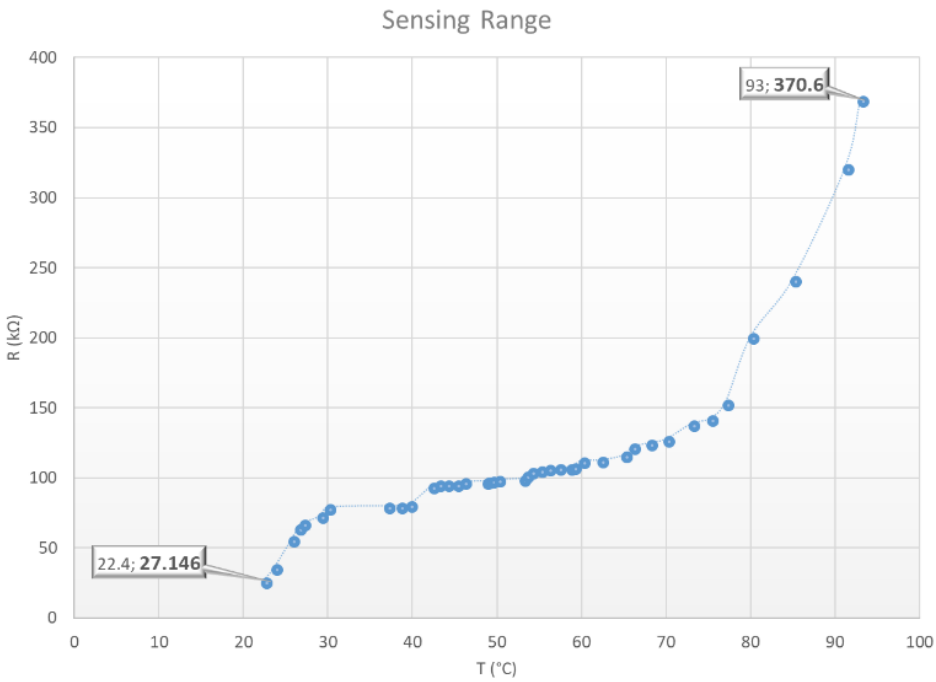

Figure 5.5 : ITO RTD response

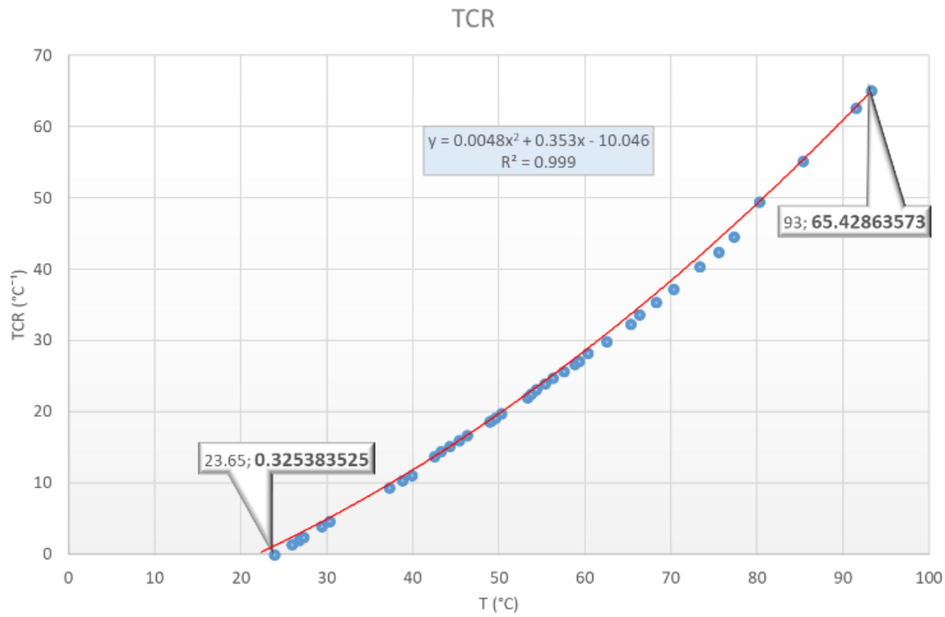

Figure 5.6 : ITO Heater TCR

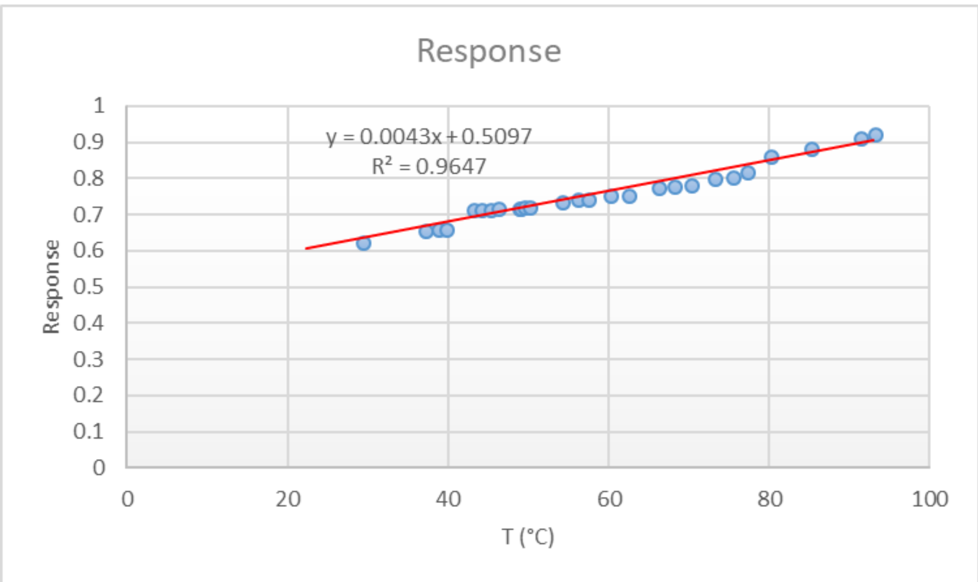

Figure 5.7 : ITO RTD normalized response

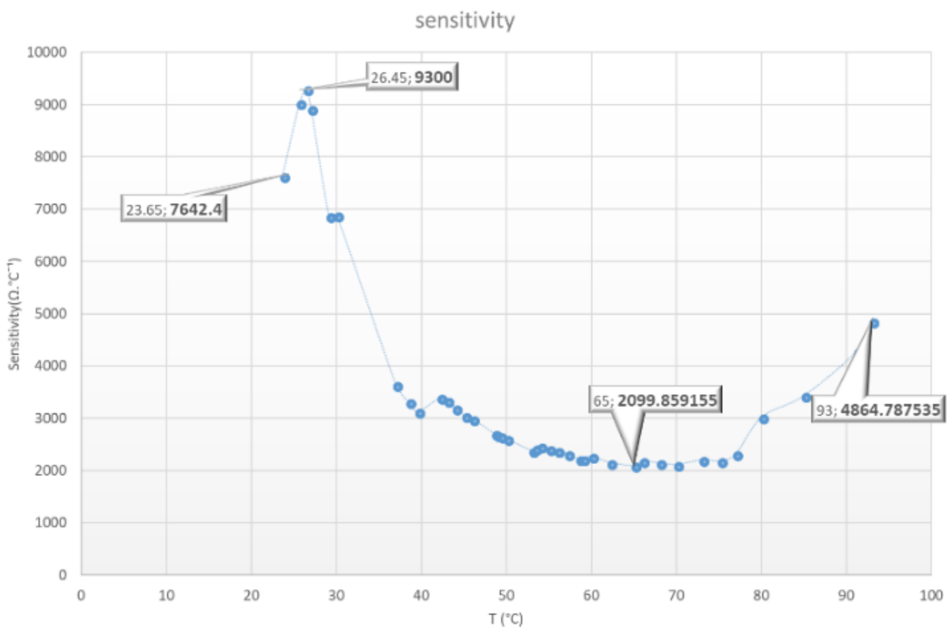

Figure 5.8 : ITO RTD sensitivity

As it is shown by the experimental results, the heater/thermal sensor created in this thesis present not only high responses to a change as small as 0.1ºC (Figure 5.5) with high TCR(5.6), but also selective sensitivity depending on the temperature range observed (Figure 5.8). The causes of these results will be explained in the following section.

5.3 Effects of Diffusion on RTD sensitivity

In this thesis, the common performance of our ITO RTD system was enhanced using mainly by doping the ITO material used for RTD patterning.

5.3.1 Semiconductor doping for enhanced sensitivity

It is necessary to first state that ITO, is a heavily doped semiconductor or degenerate semiconductor which has a behavior similar to metal conductor while keeping its other semiconductor characteristics. Indeed, when the semiconductor is doped to a certain extent, The impurity atoms are close to the extent that donor/acceptor electrons/holes can interact with each other which leads the Fermi level to be included inside the band (Figure 5.9) [5.8].

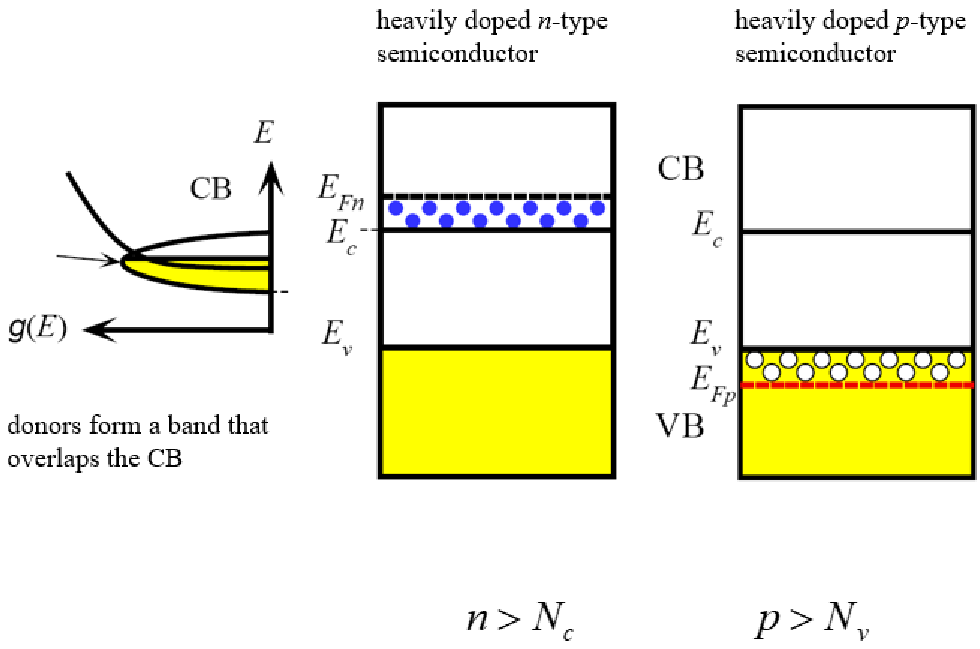

Figure 5.9 : Degenerate semiconductor energy-based characterization [5.9]

Moreover, the performance of an RTD system relies mainly on the resistivity of the material used for the sensor patterning. That resistivity can be expressed through the lattice temperature as below :

$$\rho = \frac{1}{q(\mu e(T)*ne(T)+(\mu p(T)*np(T))} \quad (5.10)$$

Where ρ is the resistivity (Ω-cm), q is the charge of the electron (C), n_e (n_p) the free electron (hole) density (cm^{-3}) in silicon, and μ_e (μ_p) is the mobility of electron (hole) (cm^2/V-s) [5.10].

Through this relation, we can see that, for heavily doped material such as degenerate semiconductors, impurity scattering has a prominent effect at low temperature. Furthermore, due to higher impurity scattering, the mobility decreases with an increase in impurity concentration for a given temperature [5.11].

Thus, since most of semiconductors operate in the saturation region (Figure 5.10), it is possible to enhance a semiconductor-based RTD sensitivity by doping the material which will change the slope of the material freeze-out zone to match the one of the intrinsic zone.

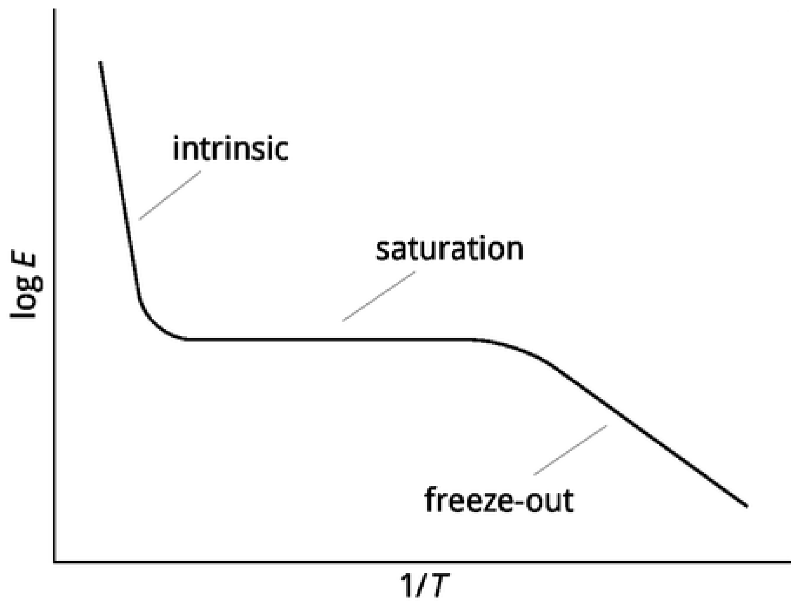

Figure 5.10 : Carrier density in doped n-type Semiconductors (similar for p-type semiconductors) [5.12]

5.3.2 Diffusion principle

The diffusion process is described as the movement of atoms from a high concentration area to a low concentration one. While liquid and gas diffusions are done through flow, solid diffusion is achieved through jumping of atoms across a fix network of sites. Furthermore, solid diffusion can be divided into two categories : the self-diffusion, in which the host atoms migrate through their own lattice, and the inter-diffusion, in which impurity atoms migrate in the host lattice. In the self-diffusion case, host atoms migrate from a normal lattice position to an adjacent vacancy through the substitutional diffusion mechanism, while in the inter-diffusion case, impurity atoms migrate from an interstitial site to a neighboring empty interstitial site which corresponds to the interstitial diffusion mechanism (Figure 5.11).

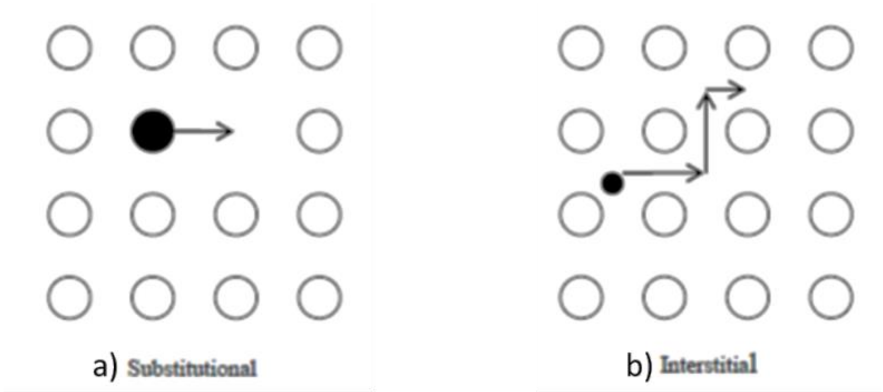

Figure 5.11 : Diffusion mechanism, a) substitutional diffusion, b) interstitial diffusion [5.11]

Moreover, Fick’s diffusion laws define two types of diffusion : the steady state diffusion which is independent of time and the non-steady state diffusion for which the diffusion rate is a function of time [5.13].

According to the first Fick law, which defines the steady state diffusion through the relation between the diffusive flux and the existing concentration gradient :

$$J = -D\frac{dc}{dx} \qquad (5.11)$$

Where J defines the diffusive flux, D is the diffusion constant and $\frac{dc}{dx}$ represents the concentration gradient.

On the other hand, the non-steady state diffusion is defined with Fick’s second law which establishes the proportionality between the rate of compositional change and the rate of concentration gradient change:

$$\frac{dc}{dt} = D\frac{d^2c}{dx^2} \qquad (5.12)$$

5.3.3 Gold and chromium diffusion mechanisms in ITO

There are generally two types of dopant or diffusers distinguished using their diffusion mechanism, thus their diffusion rate : slow diffusers, such as groups III and V diffusers, necessitate intrinsic point defects such as vacancies or self-interstitials in order to diffuse via the substitutional mechanism, on the contrary, fast diffusers, such as gold and chromium, diffuse using the substitutional-interstitial process but more predominantly the interstitial mechanism [5.14]. Indeed, substitutional-interstitial diffusion can be divided into two types of mechanism : the Frank-Turnbull mechanism (Figure 5.12a)) and the kick-out mechanism (Figure 5.12 b)).

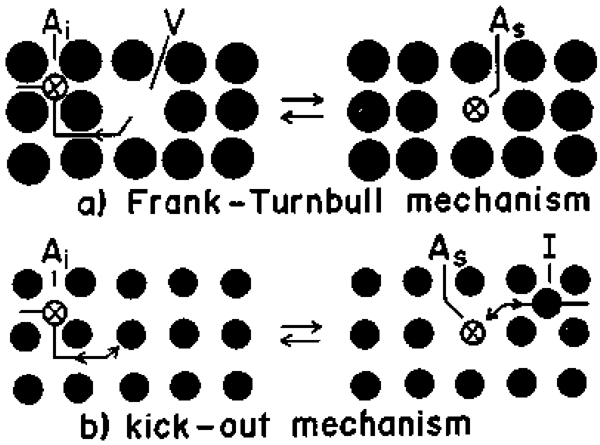

Figure 5.12 : Substitution-interstitial diffusion mechanisms, a) Frank-Turbull mechanism, b) kick-out mechanism [5.15]

As mentioned in the heater/thermal sensor system fabrication process in chapter 4, the interconnection section of the ITO-based RTD is doped first with chromium followed by another doping with gold (Figure 4.9). Chromium is first deposited through evaporation at room temperature and it diffuses into the ITO layer underneath it. Afterwards gold is also deposited by evaporation, and diffuses through the chrome layer into the ITO layer. As a result of this process, two main behaviors stood out from our RTD calibration results (Figures 5.5, 5.6, 5.8) : the high sensitivity recorded and the three-regions sensor response. Each of these two characteristics can be attributed to each of the metals used for RTD performance enhancing by doping.

On one hand, semiconductor-based RTD doping using gold is an already established process to enhance the RTD performance by improving its sensitivity [5.11]. Indeed, depending on whether an oxygen or a nitrogen ambient the RTD response will be either exponential or linear, respectively (Figure 5.13). In our study, a nitrogen ambient was used in order to allow a better monitoring of the other metal effect on the RTD performance (in this case a three region response).

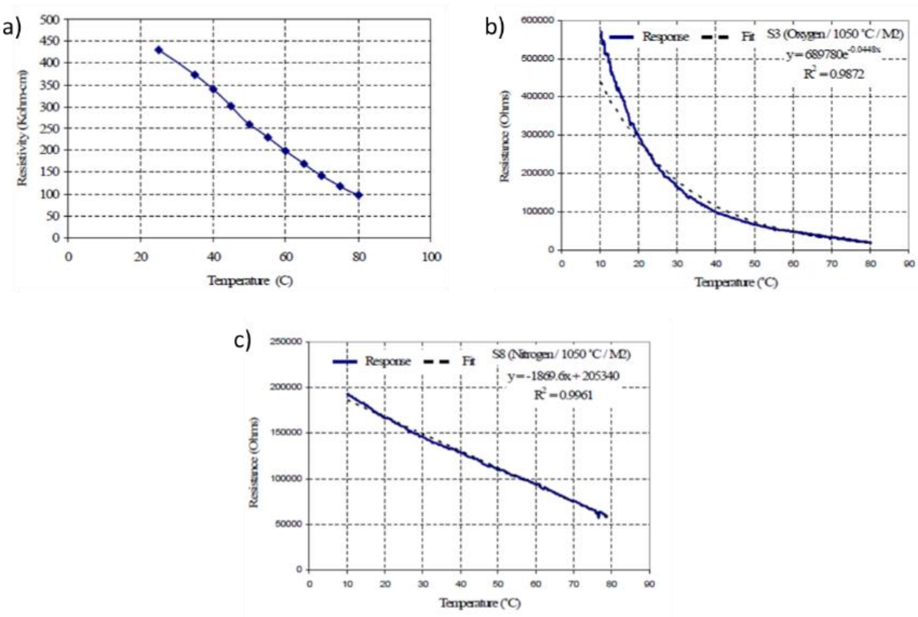

Figure 5.13 : N-type silicon-based RTD response, a) without doping, b) gold doping in an oxygen ambient, c) gold doping in nitrogen ambient [5.11]

On the other hand, semiconductor-based RTD doping using chromium is not, according to our knowledge, a well established process yet, thus the effect of chromium doping on our RTD system was defined based on empirical evidences. Therefore, we hypothesize in this thesis that chromium is responsible for the three linear regions visible in the RTD response (Figure 5.5).

5.4 References

[5.1] DropBot: An open-source digital microfluidic control system with precise control of electrostatic driving force and instantaneous drop velocity measurement Ryan Fobel, Christian Fobel, *and* Aaron R. Wheeler, Applied Physics Letters 2013 102:19.

[5.2] http://microfluidics.utoronto.ca/dropbot.

[5.3] R. Kumar and N. Sahoo, "Design, Fabrication and Sensitivity Analysis of the Resistance Temperature Detector Thin Film Sensors" International Journal of Mechanical and Industrial Engineering (IJMIE) ISSN No. 2231-6477, vol. 2, Iss-4, 2012.

[5.4] K. A. Chaudhari, FABRICATION, CALIBRATION AND CHARACTERIZATION OF MICRO-SCALE RESISTANCE TEMPERATURE DETECTORS, Master Thesis (2016).

[5.5] http://www.thermosensors.com/rtd/definitions_2.htm.

[5.6] Lee C-Y, Lin C-H, Lo Y-M. Fabrication of a Flexible Micro Temperature Sensor for Micro Reformer Applications. *Sensors (Basel, Switzerland)*. 2011;11(4):3706-3716.

[5.7] Acromag, "CRITERIA FOR TEMPERATURE SENSOR SELECTION OF T/C AND RTD SENSOR, The Basics of Temperature Measurement Using RTDs Part 2 of 3", 8500-917-A11E000 (2011).

[5.8] W. K. Chen, Electrophysics NCTU, http://ocw.nctu.edu.tw/upload/classbfs1209043550157212.pdf.

[5.9] E. Booth, " Semiconductor Industry: Increasing miniaturization (Moore's Law) is leading to Nanoelectronics".

[5.10] S. K. Gamage, N. Okulan and H. T. Henderson, "Behavior of bulk micromachined silicon flow sensor in the negative differential resistance regime", J. Micromech. Microeng., 2000, pp. 421 - 429.

[5.11] B. B. K. Premchand, "Bulk silicon based temperature sensor", Master Thesis (2005)

[5.12] http://ph.qmul.ac.uk/~anthony/spfm/24.html.

[5.13] D. Shaw, “Atomic Diffusion in Semiconductors”, Plenum press, 1973.

[5.14] U. M. Gösele, “Fast diffusion in semiconductors”, Ann. Rev. Mater. Sci., 1988, 18, pp. 257 – 282.

[5.15] Gösele, U. 1987. Proc. NATO Adv. Study Inst. on Microelectronic Materials and Processes, 1986. Boston: Martinus Nijhoff

Chapter 6. Conclusion and Future work

6.1 Conclusion

6.1.1 Novel bead-less separation method

We designed and fabricated in this thesis, in the best of our knowledge, the first of its kind EWOD-based SELEX platform in order to overcome the issue of low throughput, time consuming and laborious characteristics of the SELEX process which impedes the raise of aptamers as the next cutting edge therapeutic tool. Notably, by using an EWOD-based DMF, it is possible to reduce the amount of reactant used, and we designed a novel aptamer-target complexes and unbound sequences separation method combining the electrophoretic mobility change principle and the Cassie/Wenzel reversible wetting transitions.

6.1.2 Phase 1 characterization : a highly sensitive RTD sensor

We created in the process an ITO-based RTD for our heating/thermal sensing system enhanced through a novel doping protocol in a nitrogen ambient. Indeed, we simultaneously doped our ITO material with two different metals, using the metal-metal inter-diffusion process, each triggering a specific modification of the RTD performance characteristics. On one hand, by doping with gold, the RTD response was increased drastically compared not only to other ITO-based RTD developed so far (Figure 6.1), but also compared to other gold doped semiconductor-based RTD in nitrogen ambient (Table 6.1) regarding the doped surface area. Our dopants were deposited only in the interconnection area (1,47mm x 1,27mm) in order to avoid the possible corrosion issues among others.

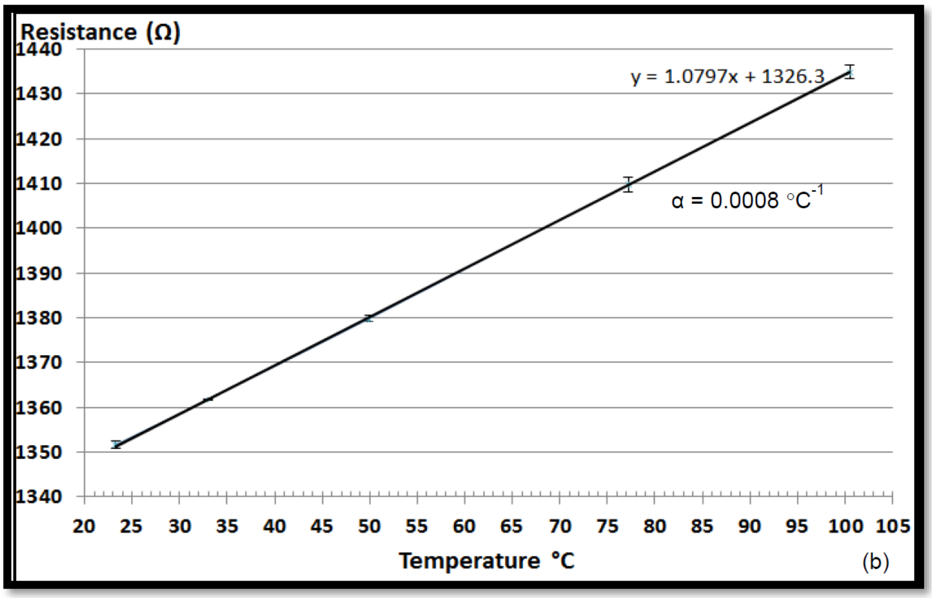

Figure 6.1 : Common ITO-based RTD response [5.4]

Sample	Diffusion Parameters (Ambient/°C/Mask)	Linear Equation R=f(T)	Accuracy (%)	Sensitivity (Ω/°C)
S6	N_2 / 1000 / M2	R = -733.93T + 86220	97.98	733.9300
S7	N_2 / 1050 / M1	R = -2736.2T + 341676	97.54	2736.2000
S8	N_2 / 1050 / M2	R = -1869.6T + 205340	99.61	1869.6000
S9	N_2 / 1050 / M3	R = -7.1141T + 1258.1	98.42	7.1141
S10	N_2 / 1100 / M2	R = -2832.3T + 331694	98.33	2832.3000

Table 6.1 : Response of n-type silicon-based RTD doped with gold in a nitrogen ambient, doped area : M1-> 10mm x 5mm, M2-> 10mm x 2mm-> 5mm x 2mm [5.11]

On the other hand, by doping with chrome, we were able to produce a RTD with a three-linear-regions-based response, with each region being used for different ranges of temperatures with a significantly high sensitivity going from 2099,86 $\Omega.^{0}C^{-1}$ to 9300 $\Omega.^{0}C^{-1}$.

6.1.3 Complete automation

A complete automation of the platform was also achieved using the DropBot system thus guarantying with the other features developed for this platform, a high throughput, efficient, time and reagent saving and with no constant user interaction needed during the whole SELEX process.

6.2 Future work : Phase 2 characterization

In the scope of this Master thesis, we limited our EWOD-based SELEX device characterization to the phase 1 which focuses on the heating/thermal sensing system calibration and characterization. The second phase of characterization, mainly covering several biological characterizations mentioned below, can be carried on as a future work goal leading to a more comprehensive study of this device.

6.2.1 Biocompatibility test

In this phase 2 characterization, biocompatibility tests will be run first to confirm that the different material used to fabricate this platform are suitable for the SELEX process through an empirical monitoring.

6.2.2 DNA/RNA/target Mixing rate calibration

As mentioned in chapter 4, the electrophoretic mobility changes depends on the target used and on whether it slows down or accelerates the aptamer-target migration velocity. Thus it is necessary to run electrophoretic mobility change monitoring for several target in order to adapt in advance the electrowetting-based micro actuation automated protocol accordingly.

6.2.3 Separation test

Furthermore, after the electrophoretic mobility change monitoring, our novel separation protocol will be tested with actual oligonucleotides sequences and previously tested targets.

6.2.4 Overall SELEX process run-test

Finally, the whole SELEX process will be run afterwards with various actuation velocities and various targets in order to determine the characteristic empirical duration of each specific protocol.

초 록

압타머는 3 차원 구조의 짧은 DNA, RNA 또는 펩타이드로 종래의 항체로는 진단이 어려운 분자나 단백질에도 높은 결합력과 특이성을 보인다. 이 '화학적 항체'는 기능적으로 기존의 항체와 유사할 뿐만 아니라 유연한 구조, 작은 크기, 높은 특이성 및 안정성 등의 장점을 가지고 있어, 질병의 변천에 대응할 수 있고 미지의 진료 기법을 개척하는 첨단 기술로 부상하고 있다. 이러한 압타머는 지수적 농축에 의한 리간드의 계통 진화(Systematic Evolution of Ligands by Exponential Enrichment, SELEX)라는 체외 분류 및 증폭 기법으로 생산되며, 수 회의 복합적인 체외 화학 반응이 수반된다. 또 제조 공정 중 지속적인 인력에 의한 오염의 위험이 있으며, 긴 제조 시간과 시약 낭비 등의 문제점이 있어 진단 및 치료 분야에서 압타머의 광범위한 활용을 저해하는 장벽으로 자리잡고 있다. 따라서 다양한 목표 물질에 적용 가능한 고속·고효율·전자동 미세유체기반 SELEX 플랫폼이 요구된다.

본 논문은 새로운 EWOD (Electrowetting-on-dielectric) 디지털 미세유체 플랫폼 기반 자동화 SELEX 시스템을 제시한다. 최신 미세 전자 기계 시스템 (Microelectromechanical systems, MEMS) 제작 기술을 활용하여 SELEX 과정에 요구되는 가열, 혼합 및 분리 등 다양한 통합 기능을 EWOD 플랫폼 상에 구현한다. 본 EWOD 플랫폼은 SELEX 전 과정이 하나의 물방울 내에서 진행될 수 있도록 디자인 되었고, 물방울은 여러 반응 부로 옮겨지면서 기존의 SELEX 과정과 같은 반응 조건을 거치게 된다. 이러한 물방울의 움직임은 물방울과

유전체의 양단에 인가된 전압으로 물방울의 표면과 접촉각을 변화시키는 전기적 인터페이스에 의해 구현된다.

본 연구는 총 3 단계로 구성되며, 그중 두 단계가 본 석사 과정 내에 진행되었다. 1 단계에서 SELEX 를 위한 EWOD 디지털 미세 유체 플랫폼이 제작되었고, 2 단계에서 SELEX 과정의 정밀한 열 제어를 위한 고성능 RTD (Resistance thermal detector) 히터/센서 시스템의 설계 및 성능 분석이 진행되었다. 3 단계에서는 개발된 플랫폼의 생물학적 실험 및 SELEX 전 단계 검증이 실행될 것이다.

본 시스템의 구상과 1 차 성능 특성 분석 단계에서 저항가열과 RTD 원리를 기반으로 한 고성능의 가열/센싱 시스템을 개발하였다. Indium tin oxide (ITO)를 다양한 물질로 도핑하여 전기적인 특성을 변환하였다. 문헌 상 기록된 값에 비해 수 천에서 수 만 배 높은 저항온도계수를 포함하는 등 독특한 성질을 가진 센서를 개발하였다.

주요어: 압타머, SELEX, RTD, EWOD, TCR, MEMS
학 번: 2016-28096